Semi Annual Report

(July 1 — December 31, 1999)

Contract Number NAS5—31363

OCEAN OBSERVATIONS WITH EOS/MODIS:

Algorithm Development and Post Launch Studies

Howard R. Gordon
University of Miami
Department of Physics
Coral Gables, FL 33124
(Submitted January 15, 2000)

Preamble

This document describes our progress thus far toward completion of our research plans regarding two MODIS Ocean-related algorithms.

A. Retrieval of the Normalized Water-Leaving Radiance (Atmospheric Correction).
B. Retrieval of the Detached Coccolith/Calcite Concentration

Our plans for Fiscal Year 2000 are included in this report as Appendix 1. Fiscal Year 2000 was to be heavily focused on validation of MODIS-derived products. Unfortunately, the delay of the launch of Terra requires some modification of out initial plan. Our approach is to use SeaWiFS for *validating* MODIS *algorithms* in the absence of MODIS itself, and when MODIS data become available, to perform the required initialization exercise and validate the MODIS products directly. However, as we already know (from theoretical studies and from SeaWiFS), that there are certain situations in which the algorithms are unable to perform properly, or that there are items that have not been included in the initial implementation, a portion of our effort will be directed toward algorithm improvement. Thus, we break our effort into two broad components for each algorithm:

- Algorithm Improvement/Enhancement;
- Validation of MODIS Algorithms and Products.

Of course, these components will overlap in some instances.

RETREIVAL OF NORMALIZED WATER-LEAVING RADIANCE (ATMOSPHERIC CORRECTION)

Algorithm Improvement/Enhancement

1. Evaluation/Tuning of Algorithm Performance

Task Progress:

This task cannot be started until Terra is actually launched and MODIS data become available. We expect that this will be a major portion of our effort for the next reporting period.

Anticipated Future Actions:

We have made preparations to start the evaluation (see **Appendix 1**) as soon as level 1 data are available.

2. Implement the Initial Algorithm Enhancements

The most important enhancement we are considering focus on absorbing aerosols. These constitute an important unsolved atmospheric correction issue for case 1 waters, and these aerosols have a significant impact in many geographical areas. Two important situations in which absorbing aerosols make an impact are desert dust and urban pollution carried over the oceans by the winds. In the case of urban pollution the aerosol contains black carbon and usually exhibits absorption that is nonselective, i.e., the imaginary part of the refractive index (the absorption index) is independent of wavelength. In contrast, desert dust absorbs more in the blue than the red, i.e., the absorption index decreases with wavelength.

Task Progress:

We are in the process of extensively examining two enhancements: (1) the spectral matching algorithm (SMA) [Gordon, Du, and Zhang, "Remote sensing ocean color and aerosol properties: resolving the issue of aerosol absorption," *Applied Optics*, **36**, 8670-8684 (1997)]; and (2) the spectral optimization algorithm SOA [Chomko and Gordon, "Atmospheric correction of ocean color imagery: Use of the Junge power-law aerosol size distribution with variable refractive index to handle aerosol absorption," *Applied Optics* , **37**, 5560-5572 (1998)]. Simulations reveal that both algorithms have the potential to perform well in the presence of strongly absorbing aerosols.

The SMA requires a set of realistic aerosol models. In contrast, the SOA models the aerosol using a single-parameter power-law distribution with constant refractive index.

In the case of urban pollution, we expect the SOA to be more appropriate because the absorption index is assumed implicitly to be constant.

Both algorithms have been installed within our own image processing environment, and a limited set of aerosol look up tables (LUTs) have been prepared so a few test images could be processed and evaluated.

The Spectral Optimization Algorithm.

We tested the SOA using imagery off the U.S. East Coast (the Middle Atlantic Bight and Sargasso Sea). In this region, the aerosol often originates from the U.S. and is often absorbing. In this study, we examined two SeaWiFS images from October 1997: days 279 and 281 (October 6 and 8). True color renditions of these images are presented in **Figure 1**. For day 279, the atmosphere over the area examined is very turbid, while day 281 is characterized by a very clear atmosphere. Although we have no surface truth for these images, atmospheric correction in a clear atmosphere is not difficult, i.e., we expect that both the SOA and the Gordon and Wang algorithm (GW) [Gordon and Wang, Retrieval of water-leaving radiance and aerosol optical thickness over the oceans with SeaWiFS: A preliminary algorithm, *Applied Optics*, **33**, 443—452 (1994)] will perform well on day 281. Because of the turbid atmosphere on day 279, this will not be the case. Here we judge the efficacy of the algorithms under three criteria.

> First, both GW and SOA should provide similar pigment concentrations and water-leaving radiances on day 281. In the Sargasso Sea, the water-leaving radiances should be characteristic of those in clear ocean water [Gordon and Clark, Clear water radiances for atmospheric correction of ocean color scanner imagery, *Applied Optics*, **20**, 4175—4180 (1981)], particularly in the green (555 nm).
>
> Second, the retrieved pigment concentrations and water-leaving radiances for days 279 and 281 should be very similar, because we do not expect large changes in water properties over this large area at this time of the year over a time period of 48 hours. (However, note that such changes would be possible in the spring.) Local changes are possible through advection, and these are easily recognized in the imagery, but the gross values of these parameters should not change.
>
> Third, features in the water that are clearly advected, e.g., recognizable eddies, should not exhibit significant changes in pigment concentration.

Figures 2 and **3** provides imagery of the retrieved phytoplankton pigment concentration for this two days processed with the SOA ("SpectOptim") and the GW ("Standard") algorithms. (Also included is the SMA applied to day 279 using the same candidate aerosol model set as the GW algorithm.) In **Figure 2** the color scale has been chosen so that the eddy structure in the Sargasso Sea is enhanced, while in **Figure 3** the color scale emphasizes the finger-like patterns near the north wall of the Gulf Stream. In all cases,

the color scale is the same for GW and SOA. Black in the image is either clouds or land, with the exception of the black area on day 279 in the GW algorithm that does not appear in the SOA, that is not processed by the GW algorithm because the radiance at 865 nm is too large.

It is obvious that the SOA-retrieved pigment concentration is very similar in all areas for the two days. In contrast, the GW-derived concentrations differ significantly from 279 to 281, especially in the vicinity of the higher aerosol concentrations.

In the SOA, recognizable eddies in the Sargasso Sea appear to retain their pigment concentrations over the two days, while in the GW processing it is difficult to even recognize eddies there. It is interesting that there appears to be much more detail and less noise in the imagery processed with the SOA than the GW algorithm. There are two reasons for this. First, the SOA employs all of the bands to estimate the pigment concentration (and simultaneously perform atmospheric correction) as opposed to only the 490 and 555 nm bands in the standard processing. Using more bands, and wider spacing between bands, results in a noise reduction [R. Frouin, personal communication]. Second, the bands at 412 and 443 nm are significantly more sensitive to changes in pigment concentration than the 490 nm bands.

In the Sargasso Sea, the GW pigment concentration is usually higher than the SOA. This is to be expected because the SOA uses the Gordon *et al.* radiance model [Gordon *et al.*, "A semi analytic radiance model of ocean color," *Jour. Geophys. Res.*, **93D**, 10909—10924 (1988)]. Given the same spectrum of water-leaving radiances, the radiande model will yield a lower pigment concentration than the OC2 algorithm [O'Rielly *et al.*, "Ocean color chlorophyll algorithms for SeaWiFS," *Jour. Geophys. Res.*, **103C**, 24937—24953 (1998)] used in the standard processing, when the concentration is small. This difference decreases as the pigment concentration increases. Thus, we believe that the differences in the overall pigment concentrations in the Sargasso Sea are *not* the result of atmospheric correction.

The Spectral Matching Algorithm

In the case of wind-blown dust, the SOA, as presently configured, cannot produce acceptable results in the presence of wind-blown dust, because the absorption index is assumed to be constant. For atmospheric correction in dust we are attempting an alternate approach: develop realistic models of the dust (size-refractive index distributions) and apply these using the SMA. To develop a suitable dust model, we extracted a track from a single SeaWiFS image (**Figure 4**) that showed a high concentration of Saharan dust, and compared the aerosol component of the reflectance with that predicted by several aerosol models. Moulin *et al.* ["Long-term daily monitoring of Saharan dust load over ocean using Meteosat ISCCP-B2 data 2. Accuracy of the method and validation using Sun photometer measurements," *Jour. Geophys. Res.*, **102D**, 16959—16969 (1997)] showed that for the broad-band sensor on Meteosat the tri-modal background desert dust model of Shettle ["Optical and Radiative Properties of a Desert Dust Model," *Proceedings of the Symposium on Radiation in the Atmosphere*,

Ed. G. Fiocco, Deepak, Hampton, VA, 74—77 (1984)] better than a variety of other popular models. Thus, we started with his model, but to provide a better fit in the blue and violet, we used the absorption index suggested by Patterson ["Optical Properties of Crustal Aerosol: Relation to Chemical and Physical Characteristics," *Jour. Geophys. Res.*, **86C**, 3236—3246, (1981)]. The concentration, vertical extent, and relative concentration of the large-size mode of the size distribution of the dust were varied and a relationship between the aerosol contribution to the TOA reflectance at any wavelength and that at 865 nm was developed. We found that this model (which we call BDS) fit the SeaWiFS data reasonably well in many cases, but there were indications that the Patterson absorption index was too large. Thus we developed a similar model that used Shettle's size distribution, but with a smaller absorption index than Patterson's. We called this BDB. We examined 40 separate images with high concentrations of dust and found that this set (BDB and BDS with variable vertical extent) seems to fit most cases, at least near the source region. A detailed report of this work is attached as **Appendix 2**.

These models were used to make LUTs for operation of the SMA. **Figure 4** is the TOA radiance at 865 nm showing a dust event on October 3, 1997 (day 276) off the African coast. The result of processing the SeaWiFS imagery on this day with the GW algorithm (with a flag, that prevent processing in regions with high aerosol concentrations, disabled) and the SMA using the BDS models are provided in **Figure 5**. For comparison**,** result of processing the image from day 283, which was free of dust, is also provided in **Figure 5**. Clearly, the SMA is capable of retrieving realistic pigment concentrations through significant quantities of Saharan dust, where the GW algorithm fails completely.

Anticipated Future Actions:

For most of the imagery we have tested using the SOA and SMA algorithms, there has been little or no surface truth. We plan to rectify this by using imagery acquired simultaneously with surface measurements during INDOEX, in which we participated during the winter and spring of 1999. We have many of the surface measurements and the corresponding satellite imagery available, and need only to complete the required LUTS to start a more in-depth analysis of the efficacy of these algorithms. The INDOEX study area presented aerosols from sources that included clean maritime, desert dust, and anthropogenically polluted. This should provide a valuable validation test for these algorithms.

In addition, we need to streamline these algorithms in order to reduce the required processing time. However, this will be considered only after the evaluation of the algorithms in terms of their ability to provide meaningful derived products.

We are in the process of preparing papers describing these initial tests of the SOA and SMA (dust) algorithms.

3. Study Future Enhancements

There are three additional issues that we are examining for inclusion into the MODIS algorithm: modeling the subsurface upwelling BRDF, understanding the influence of colored dissolve organic matter (CDOM) on the operation of the SOA and SMA, and the influence of whitecaps on the sea surface.

Task progress:

The subsurface upwelling BRDF

Our attempts to precisely model the BRDF have met with limited success. In the principal plane of the sun, our models have good agreement with measurements in the same azimuth as the sun, but much poorer agreement in an azimuth opposite to the sun (precisely where an instrument such as SeaWiFS (and to a lesser extent MODIS) is designed to view. We need to understand the source of this disagreement.

During this reporting period we have proceeded with our effort to understand the ocean's BRDF. First, we have made many additional measurements of the BRDF under a variety of conditions (see Section 5 below). Second, we are collaborating with J.P. Doyle of the JRC, Ispra, Italy to model the self-shading characteristics of our radiance distribution camera system. Preliminary results suggest that shadowing may be a problem even in the blue region of the spectrum at low pigment concentrations. This is unexpected. Third, we are adding the effects of polarization to our in-water radiative transfer code.

The influence of CDOM on the SOA and SMA

No work was carried out on this problem during the present reporting period.

Influence of whitecaps on the sea surface

We completed our revision of our paper on the augmented reflectance of the sea surface in the presence of whitecaps. It has now been accepted for publication in *JGR*. The principal result is that the augmented reflectance of whitecaps in the visible is well described with the formula, $RSAR = 3\times10^{-6}U^{2.55}$, where *RSAR* is the remote sensing augmented reflectance (increase in reflectance of a pixel over the background reflectance of the water due to the presence of whitecaps) and *U* is the wind speed in m/s. In the NIR at 860 nm the *RSAR* is about 20% lower. This equation appears to describe the *RSAR* for wind speeds up to 12 m/s in the Pacific trade winds where the fetch and duration are essentially infinite. This has been relayed to the SeaWiFS Project for inclusion into the processing.

Anticipated Future Actions:

The subsurface upwelling BRDF

We will reduce the new BRDF data, and compare it with our model. We will continue the collaboration with Doyle, and the addition of polarization to our model. To study the self-shading experimentally, we will participate in Dennis Clark's February cruise and compare the measurements from RADS with those from a new smaller instrument Dennis Clark is developing for MOBY. It will have a greatly reduced self-shading problem.

The influence of CDOM on the SOA and SMA

This will be studied as time permits during the next reporting period.

Influence of whitecaps on the sea surface

This work is now essentially complete. We will now operate the whitecap instrumentation only during validation cruises.

Validation of MODIS Algorithms and Products

4. Participate in MODIS Initialization Campaign

During calendar year 1999, we participated in three major field campaigns aimed a validating various aspects of MODIS algorithms using SeaWIFS: Aerosols99, INDOEX, and MOCE5. This was a significant effort representing 105 man days actually at sea, 0 man days loading, setting up equipment, and unloading the ships, as well as significant time for performing pre- and post-cruise calibrations. This effort will continue into FY 2000.

Task Progress:

We are preparing for the field campaign that will commence within approximately 90 days of Terra's launch. Along with this preparation we participated in the MOCE-5 cruise (see section 5 below).

We have also maintained our CIMEL station in the Dry Tortugas during this period. This station will be used to help validate the MODIS derived AOD and aid in the investigating the calibration of the near infrared (NIR) spectral bands of MODIS.

Anticipated future efforts:

We will participate on the MODIS initialization campaign when Terra is launched and the cruise dates are firmed up. We will be making the same suite of measurements made on the MOCE-5 cruise (see 5 below). In addition we are working to get the Micro-Pulse lidar system operational for this cruise effort. This cruise will probably dominate our experimental efforts for at least the next reporting period.

5. Participate in Validation Campaign (SeaWiFS)

Task Progress:

During this period we participated in the MOCE-5 cruise during October (10/1/99-10/21/99). For this cruise we fielded the Sky Radiance camera system, Aureole camera system, In-Water Radiance distribution camera system (RADS), and Whitecap radiance camera. There were 20 in-water RADS casts, 19 Sky and Aureole system data sets, 12 Langley measurements with a Microtops sunphotometer, and numerous individual Microtops measurements. While the whitecap instrument was deployed several times, the whitecaps were never numerous enough to warrant even reducing this data. The rest of the data has been reduced to calibrated images, and extracted almucantor and principal plane data sets. We are now investigating this data, trying inversion routines, to look at the optical properties of the aerosols. The rest of this period was basically spent doing the pre- and post calibrations for the MOCE-5 effort.

Anticipated future efforts:

We will be looking at the reduced data sets obtained from this cruise during the next reporting period. The in-water pigment concentrations varied greatly during this cruise, giving us a large range of conditions for our BRDF measurements. These data will be very useful for helping with our modeling efforts of the in-water BRDF.

Sky conditions were the best we have had for many of our sky radiance measurements, also the ability to perform numerous Microtops langley plots gives us great confidence in the aerosol optical depth measurements for this data set. We will be using the combined sky radiance/polarization measurements to look at inversions to get the aerosol scattering properties.

For the next period we plan on supporting the validation efforts when Terra does launch. This may involve a short cruise in February 2000, and a longer cruise in April or October, 2000. These factors will be determined by the true timing of the launch. During February, we will concentrate on BRDF measurements.

The Micro-pulse lidar was not used during the MOCE-5 cruise. During the pre cruise calibration the detector failed and it could not be repaired before the cruise. There is a shortage of these detectors, but we have managed to get the manufacturer to agree to

repair the detector. Our goal is to have this system working in time for the early cruises after Terra has been launched.

RETRIEVAL OF DETACHED COCCOLITH/CALCITE CONCENTRATION

Algorithm Evaluation/Improvement

Task Progress:

A second manuscript on our Arabian Sea results is almost completed at the time of this writing. This manuscript specifically deals with the calibration of the acid-labile backscattering versus suspended calcite relationship in this region of known coccolithophore production and sedimentation. Data are presented on calcite backscattering, ranging from highly controlled lab measurements to field campaigns in the Straits of Florida, Arabian Sea, and North Atlantic Ocean. Moreover, the first continuous record of particulate inorganic carbon and particulate organic carbon, measured over ~3500 kilometers of ship track, is presented in this paper.

Anticipated future efforts:

At present, we have no detailed plan of algorithm improvement because the non-availability of sampled coccolithophore blooms in the SeaWiFS era has prevented a through testing of the algorithm. As blooms are sampled contemporaneously with MODIS imagery, the processing algorithms will be fine tuned.

Validation of MODIS Algorithms and Products

Task Progress:

In the last 1/2 year, we have logged 28 days at sea in the Gulf of Maine, making measurements of inherent optical properties (IOP's), apparent optical properties (AOP's) calcite-specific backscattering, coccolith concentration, and suspended calcite concentration. Twenty of the days were aboard a ship of opportunity, the *M/V Scotia Prince*, which sails between Portland, Maine and Yarmouth, Nova Scotia. As of December 1999, all of our 1999 pre-launch cruise data (continuous underway measurements) have been processed to preliminary form, and submitted to the NASA Sea Bass data archive as tables of time, inherent optical properties and apparent optical properties. Discrete samples from the 1998 field season are now completely worked up, including the suspended calcite samples, which were processed by the Analytical Facility at the Scripps Institution of Oceanography, on their inductively-coupled plasma atomic absorption spectrometer.

As for the 1999 field season, discrete samples for this work have mostly been processed, except for coccolith concentration (microscopy). This last work is by far the most laborious. Above water radiance data are being checked against post-cruise Spectralon plaque calibrations which were taken twice daily. This process involves extracting the specific calibration files from the complete record, then running them through algorithms to verify the calibration. We added a Hobie Labs Hydroscat 2 to our underway sampling system. After an initial failure of the instrument's mother board, it functioned reasonably well for the remainder of the summer. This instrument provided an estimate of the wavelength dependence of backscattering (at 470 and 680 nm). This is especially important for understanding the wavelength dependence of coccolith light scattering. In November, we also performed an intercalibration experiment of the Dawn Wyatt Light Scattering Photometer, Hobie Labs Hydroscat II, and the Wet Labs Eco-VSF light scattering photometer, in conjunction with Scott Pegau and Mike Twardowski of Oregon State University. This work was just completed, and these results will be worked up in the next few months.

During the 1999 field season, a high reflectance feature was observed in the Gulf of Maine by SeaWiFS, but unfortunately, it was in Canadian waters, and permission could not be acquired fast enough to get our gear out to sample it, before it disappeared.

Anticipated future efforts:

We are involved in the planning of10 more days of ship-of-opportunity work aboard the m/s *Scotia Prince* between May and October of 2000. Moreover, in the event that a coccolithophore bloom is observed this coming summer, we are including 5 days of ship time so that we will be able to sample it. In the event no bloom is observed, we are looking into other ways of acquiring measurements of high-reflectance calcite features in the sea, which we could use for the MODIS algorithm tuning. Data from coccolithophore blooms have not been easy to acquire due to the inability to predict their occurrence in space and time. One possible solution is to spread a limited patch of pulverized cretacious chalk (consisting of ground coccoliths) in a 1-2 km^2 area in the Jordan Basin, which could then be observed by MODIS (using the 470 and 550nm, 500m resolution bands; signal to noise of ~220). We would load our shipping container/laboratory aboard a small vessel in support of shipboard optical measurements, as we created the patch, mapped it, and performed discrete measurements. In support of this work, we have included a Satlantic TSRBII spectral radiometer, for sub-surface measurements of upwelling radiance and downwelling irradiance just above the surface, at select MODIS wavelength bands. In regards to publication activities, we will complete a second *Deep Sea Research II* manuscript, and submit it for review, and then move on to writing up the Gulf of Maine algorithm work.

PUBLICATIONS

E. J. Welton, K. J. Voss, H. R. Gordon, H. Maring, A. Smirnov, B. Holben, B. Schmid, J. M. Livingston, P. B. Russell, P. A. Durkee, P. Formenti, M. O. Andreae, "Ground-based lidar measurements of aerosols during ACE-2: instrument description, results, and comparisons with other ground-based and airborne measurements", *Tellus*, (In press).

B. Schmid, J. M. Livingston, P. B. Russell, P. A. Durkee, H. H. Jonsson, D. R. Collins, R. C. Flagan, J. H. Seinfeld, S. Gassó, D. A. Hegg, E. Öström, K. J. Noone, E. J. Welton, K. J. Voss, H. R. Gordon, P. Formenti, and M. O. Andreae, "Clear sky closure studies of lower tropospheric aerosol and water vapor during ACE 2 using airborne sunphotometer, airborne in-situ, space-borne, and ground-based measurements", *Tellus*, (In press).

J. M. Ritter and K. J. Voss, A new instrument to measure the solar aureole from an unstable platform, *Journal of Atmospheric and Oceanic Technology*, (Accepted).

K.D. Moore, K. J. Voss, and H. R. Gordon, "Spectral reflectance of whitecaps: Their contribution to water leaving radiance", *Journal of Geophysical Research*, (Accepted).

Balch, William M., David T. Drapeau, Terry L. Cucci, and Robert D. Vaillancourt, Katherine A. Kilpatrick, Jennifer J. Fritz. 1999. Optical backscattering by calcifying algae-Separating the contribution by particulate inorganic and organic carbon fractions *Jour. Geophys. Res.* **104**, 1541—1558.

Vaillancourt, R. D. and W. M. Balch. Size distribution of coastal sub-micron particles determined by flow, field flow fractionation, *Limnology and Oceanography*.(In press).

Graziano, L., W. Balch, D. Drapeau, B.Bowler, and S. Dunford. Organic and inorganic carbon production in the Gulf of Maine, *Cont. Shelf Res.* (In Press).

Balch, W. M., D. Drapeau, and J. Fritz. Monsoonal forcing of calcification in the Arabian Sea, *Deep Sea Research II*, (In press).

Milliman, J., P.J. Troy, W. Balch, A.K. Adams, Y.-H. Li, and F.T. MacKenzie . 1999. Biologically-mediated dissolution of calcium carbonate above the chemical lysocline? *Deep-Sea Res. I*, **46**, 1653—1669.

PRESENTATIONS

C. Moulin, H.R. Gordon, V.F. Banzon, R.H. Evans, F. Dulac, C.E. Lambert, D. Tanre, Satellite remote sensing of mineral dust in the visibel from Meteosat to SeaWiFS, Workshop on Mineral Dust, Boulder, CCO, June 9--11, 1999.

E. Welton, P. Flatau, K. Voss, H. Gordon, K. Markowicz, J. Campell, J. Spinhirne, "Measurements of the vertical distribution of aerosols and clouds during INDOEX 1999 Using Micro-pulse Lidars", Poster Paper (A32B-07), 1999 AGU Fall Meeting. San Francisco, CA (December 12--17).

B. Schmid, D. R. Collins, S. Gassó, E. Öström, E. J. Welton, P. A. Durkee, J. M. Livingston, P. B. Russell, R. C. Flagan, J. H. Seinfeld, D. A. Hegg, K. J. Noone, K. J. Voss, H. R. Gordon, J. Reagan, and J. Spinhirne, Clear-sky Closure Studies of Tropospheric Aerosol and Water Vapor During ACE-2 Using Airborne Sunphotometer, Airborne in-situ, Space-borne and Ground-based Measurements, Abstract (A32E-08), 1999 AGU Fall Meeting, San Francisco, CA (December 12--17).

C. Moulin, H.R. Gordon, R.M. Chomko, V.F. Banzon, and R.H. Evans, Mineral dust observations with SeaWiFS: Dust models derived from spectral measurements, Abstract (A41F-12), 1999 AGU Fall Meeting, San Francisco, CA (December 12--17).

P.J. Flatau, G. Mitchell, A. Subramaniam, J. Wieland, E.J. Welton, K. Markowicz, J. Nelson, K. Voss, H. Gordon, R.M. Reynolds, M. Miller, T. Nakajima, K. Rutlidge, M. Kahru, Ocean Color and Aerosols, Abstract (A31E-09) 1999 AGU Fall Meeting, San Francisco, CA (December 12--17).

R. Evans, C. Moulin, P. Minnett, H. Gordon, V. Banzon, and C. Moulin, Combined use of visible and infrared channels to identify and correct African dust aerosols, Paper Number 3868--71, EUROPTO, Rome, Italy.

W. M. Balch, Drapeau, D. T., Bowler, B., Ashe, A., Vaillancourt, R., Dunford, S., and Graziano, L. 1999. Backscattering probability and calcite-dependent backscattering in the Gulf of Maine. Proceedings of the ASLO Meeting, Santa Fe, NM. *ASLO Santa Fe,* 1-5 February, 1999, p. 18.

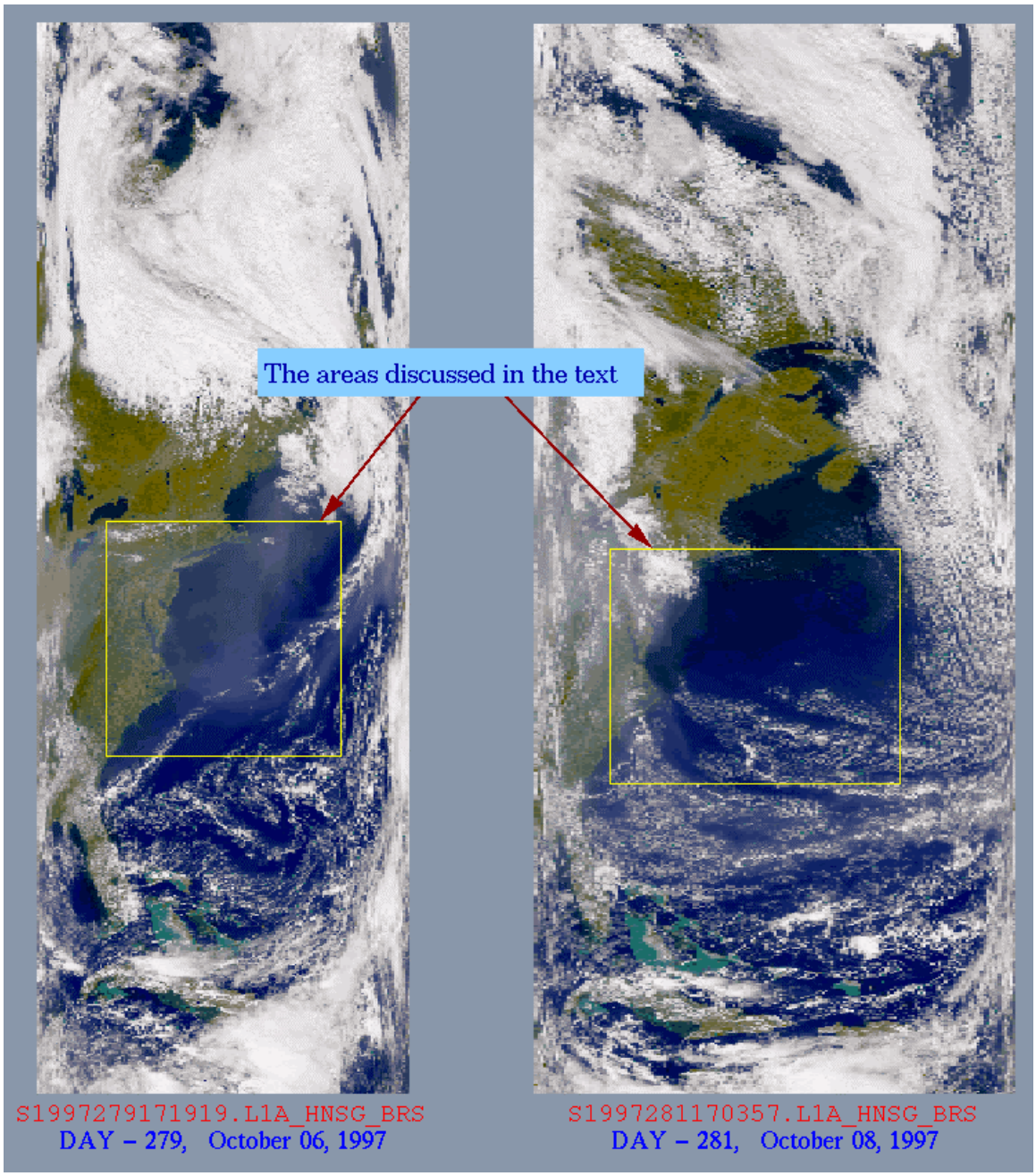

Figure 1. "True color" images taken by SeaWiFS on October 6 1997 (day 279) and October 8, 1997 (day 281) off the East Coast of the United States.

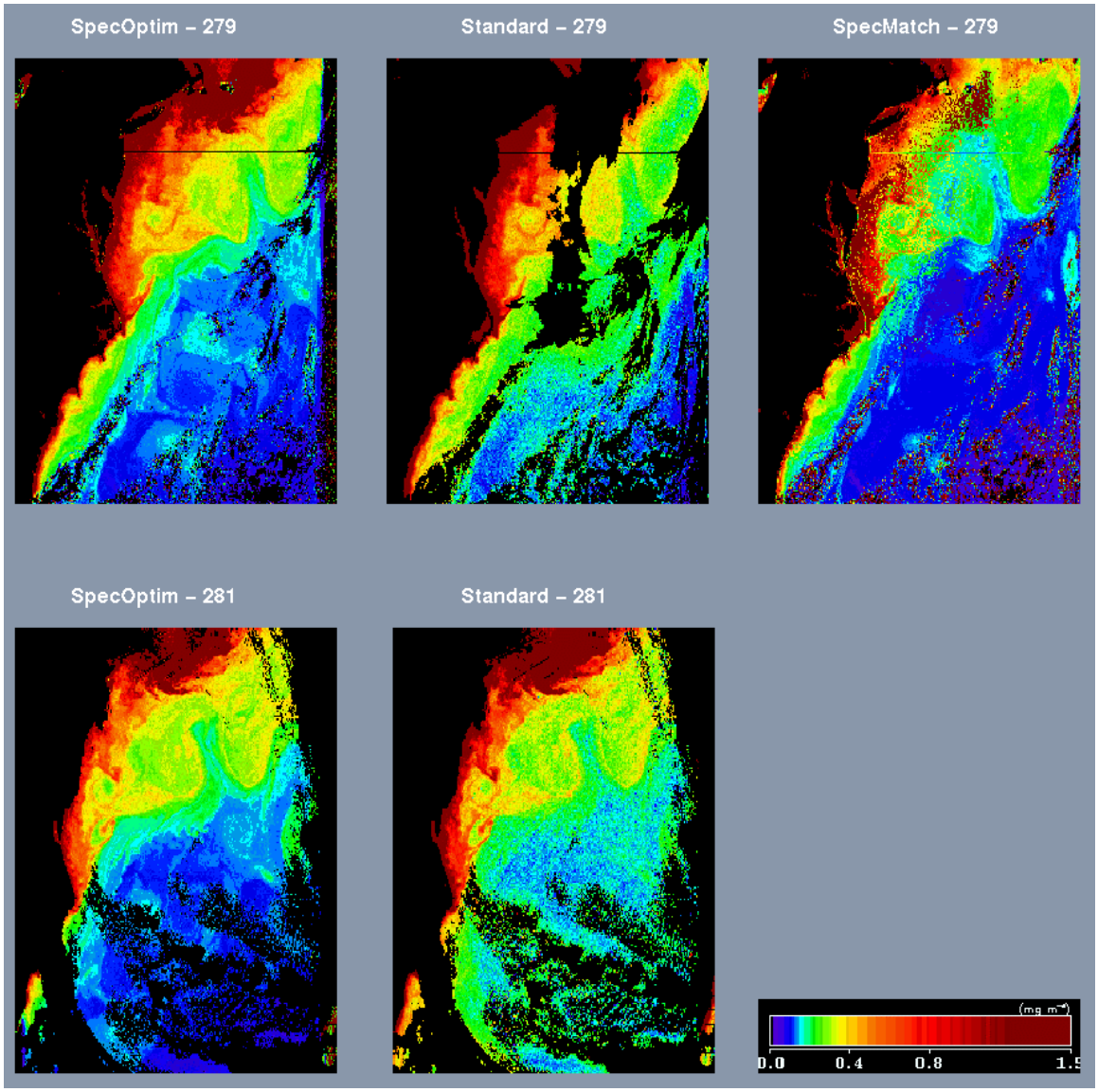

Figure 2. Comparison of the SOA ("SpectOptim") and the GW algorithm ("Standard") operating on SeaWiFS images off the U.S. East Coast for days 279 and 281 (October 6 and 8, 1997). The color scale has been chosen to enhance the eddy structure south of the Gulf Stream in the Sargasso Sea.

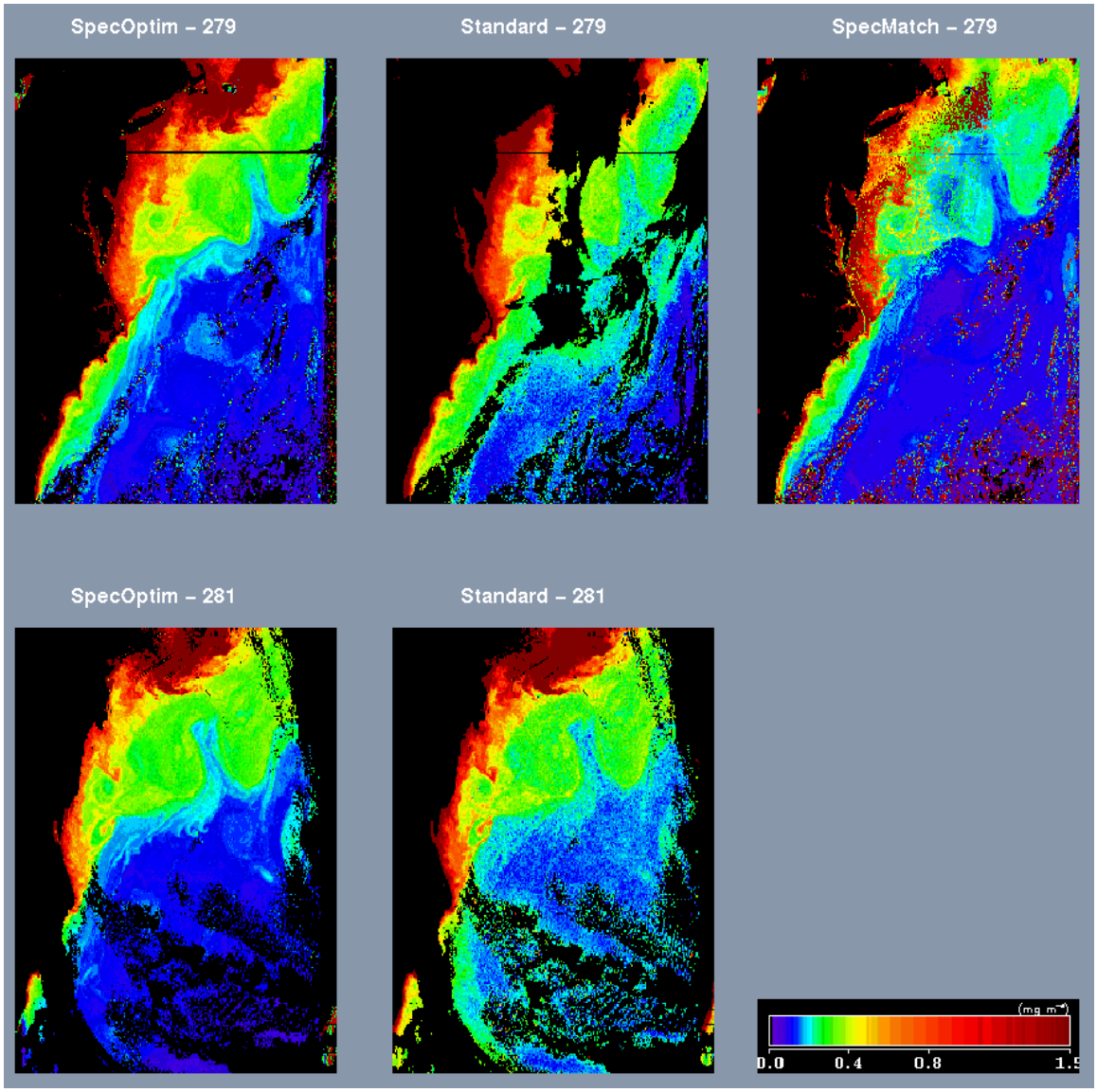

Figure 3. Comparison of the SOA ("SpectOptim") and the GW algorithm ("Standard") operating on SeaWiFS images off the U.S. East Coast for days 279 and 281 (October 6 and 8, 1997). The color scale has been chosen to enhance the finger-like patterns near the north wall of the Gulf Stream.

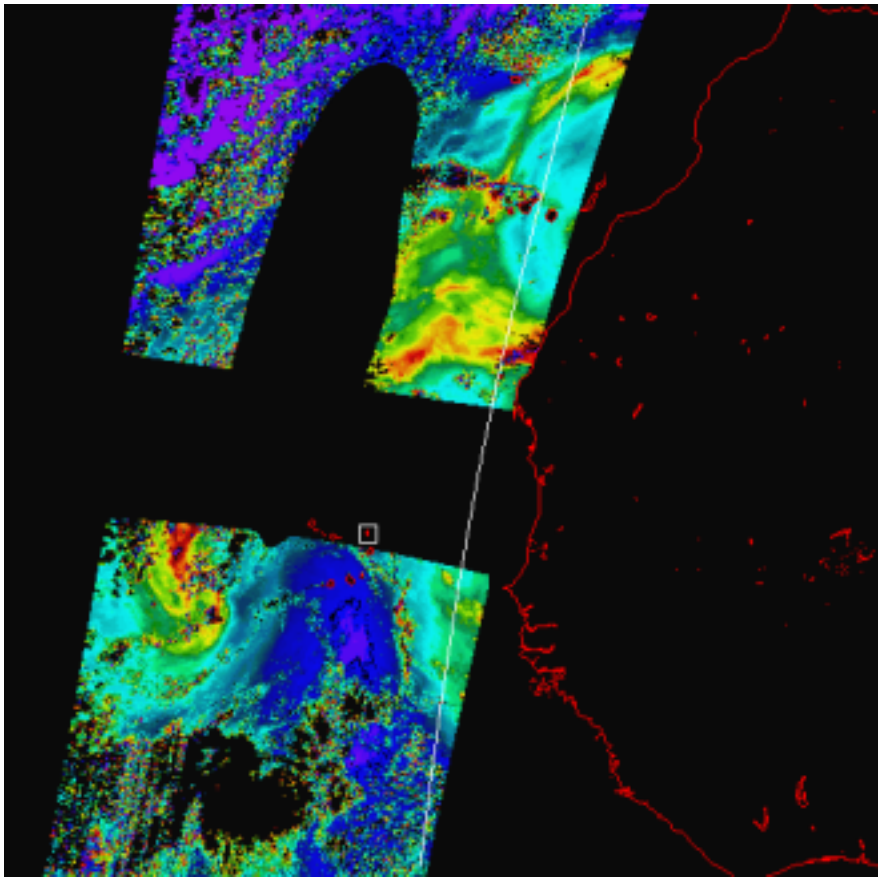

Figure 4: SeaWiFS image of the aerosol component of the reflectance at 865 nm from 98174 (year 1998, day 174). Reflectance is high for red colors and low for blue-purple. The vertical black area is the portion masked because of sun glint, and the horizontal strip is the data that is missing because of the change in the sensor's tilt from north to south.

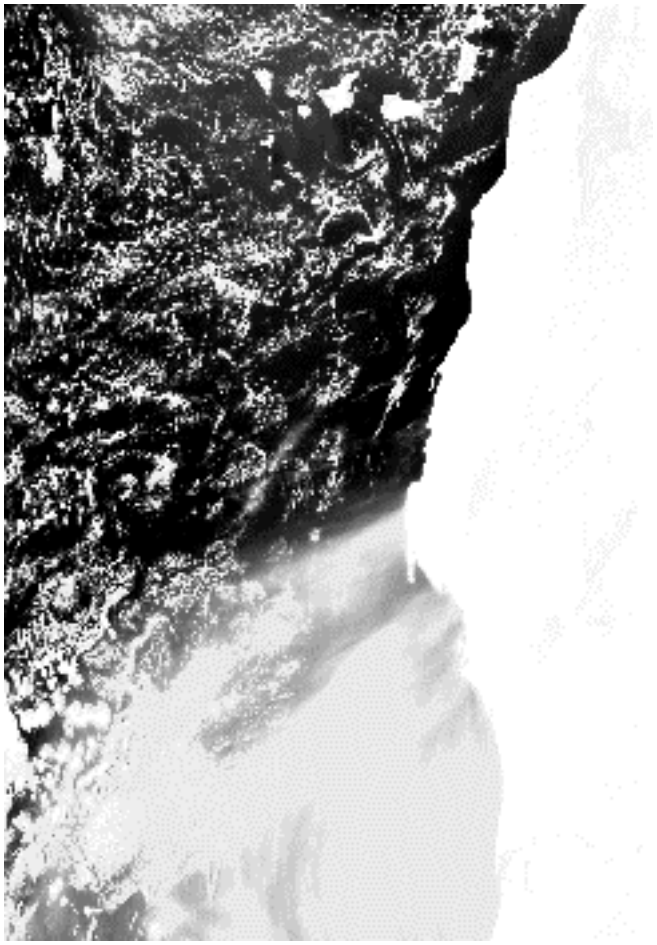

Figure 5. Level 1 (calibrated sensor radiance) SeaWiFS image at 865 nm of a dust event of the Coast of West Africa on day 276 (October 3, 1997). The hook-like coastal feature near the center of the image is Cap Blanc, Mauritania. Low radiance is dark and high radiance is white.

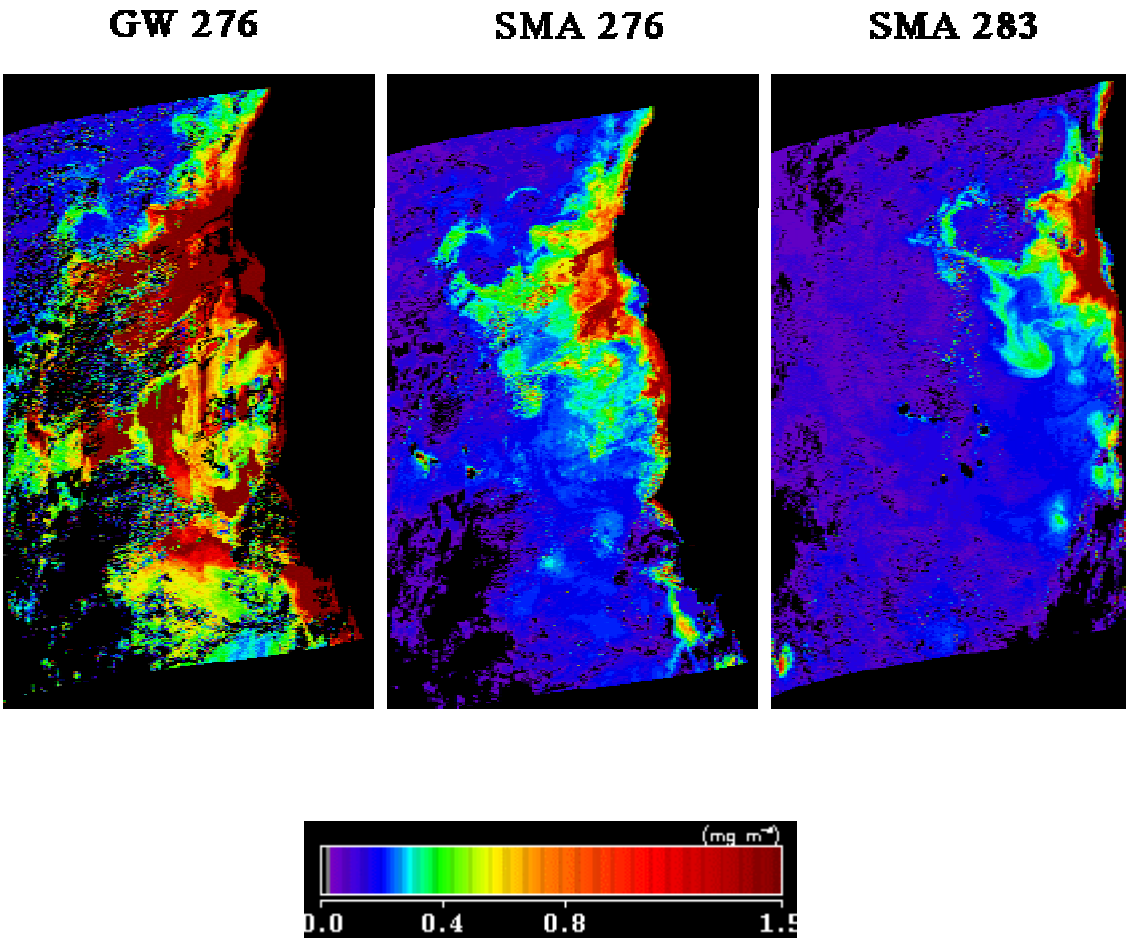

Figure 6. Pigment concentration retrieved for SeaWiFS imagery acquired off the Coast of West Africa on days 276 (October 3, 1997, and shown also in **Figure 5**) and 283 (October 10, 1997). The left panel is day 276 processed using the standard GW algorithm with flags that block processing at high aerosol concentration removed. The center panel is day 276 processed with the SMA using the BDS aerosol models. The right panel is day 283 processed with the SMA using the BDS aerosol models. There was no visual evidence of dust on day 283.

Appendix 1

NASA/GSFC Contract No. NAS5-31363

OCEAN OBSERVATIONS WITH EOS/MODIS
Algorithm Development and Post Launch Studies

Howard R. Gordon
University of Miami
Department of Physics
Coral Gables, FL 33124

Plans for FY 00

Preamble

This document describes plans for Fiscal Year 2000 regarding two MODIS Ocean-related algorithms.

A. Retrieval of the Normalized Water-Leaving Radiance (Atmospheric Correction).

B. Retrieval of the Detached Coccolith/Calcite Concentration

Fiscal Year 2000 will be heavily focused on validation of MODIS-derived products. Unfortunately, the delay of the launch of Terra requires some modification of out initial plan. Our approach for the coming year will be to use SeaWiFS for *validating* MODIS *algorithms* in the absence of MODIS itself, and when MODIS data become available, to perform the required initialization exercise and validate the MODIS products directly. However, as we already know (from theoretical studies and from SeaWiFS) that there are certain situations in which the algorithms are unable to perform properly or that there are items that have not been included in the initial implementation, a portion of our effort will be directed toward algorithm improvement. Thus, we break our effort into two broad components for each algorithm:

- Algorithm Improvement/Enhancement;
- Validation of MODIS Algorithms and Products.

These components will overlap in some instances.

RETREIVAL OF NORMALIZED WATER-LEAVING RADIANCE (ATMOSPHERIC CORRECTION)

Algorithm Evaluation/Improvement

1. *Evaluation/Tuning of Algorithm Performance*

Once MODIS imagery becomes available, there are several aspects of the data that must be examined. After the initialization procedure, with a ship-borne campaign, the imagery must be examined on a regular basis to ensure that the algorithms and the instrument are operating properly. Specifically, the sensor-algorithms should provide the expected "clear water radiances" [Gordon and Clark, "Clear water radiances for atmospheric correction of coastal zone color scanner imagery," *Applied Optics,* **20**, 4175-4180, 1981] in the blue-green region of the spectrum, and should retrieve water-leaving radiances that agree with measurements at the MOBY site [Clark *et al.*, "Validation of Atmospheric Correction over the Oceans," *Jour. Geophys. Res.,* **102D**, 17209-17217, 1997]. Any deviation from expectation or measurement must be reconciled. Deviations could be due to time dependence of the sensor calibration coefficients (i.e., instability in the sensor's radiometric response), improper initialization, improper correction for the sensor's polarization sensitivity, etc. Such analysis of necessity involves a statistical study of the derived water-leaving radiances with sufficient observations to unravel possible effects due to viewing angle, solar zenith angle, and other factors that could influence the retrievals. In addition, the performance of the atmospheric correction algorithm needs to be carefully studied. For example, does the algorithm choose candidate aerosol models that do not vary significantly from pixel to pixel? Such variation could indicate poor performance of the sensor in the NIR. Do the models that are chosen suggest that $\varepsilon(749,869)$ is undergoing a systematic variation with time? Such a variation would indicate that the radiometric response of the sensor is varying in time.

These studies will enable the algorithms to be tuned to the sensor and, in the event of an expected degradation in the sensor response, provide the necessary corrections to the response.

2. *Implement the Initial Algorithm Enhancements*

Several algorithm enhancements are planned for implementation into the processing stream in the immediate post-lanch era. Most of the enhancements focus on dealing with absorbing aerosols, which we consider to be the most important of the unsolved atmospheric correction issues because it has such a significant impact in many geographical areas. They are under intense development now. Among the enhancements we are studying are the spectral matching algorithm (SMA) [Gordon, Du, and Zhang,

"Remote sensing ocean color and aerosol properties: resolving the issue of aerosol absorption," *Applied Optics*, **36**, 8670-8684 (1997)], the spectral optimization algorithm SOA [Chomko and Gordon, "Atmospheric correction of ocean color imagery: Use of the Junge power-law aerosol size distribution with variable refractive index to handle aerosol absorption," *Applied Optics* , **37**, 5560-5572 (1998)], and application of a model of Saharan dust transported over the ocean by the winds that is currently in the testing phase (Moulin *et al.*, in preparation).

The SMA is now being studied extensively because it can be added to the present MODIS algorithm with minor impact, as it uses the same look-up-tables (LUTs) as the existing algorithm. Another attractive feature is that it is completely compatible with our present plans for dealing with wind-blown desert dust. We plan to implement this algorithm in phases. In the first phase, the algorithm will be used to provide a flag that signals the presence of absorbing aerosols. In the second phase, the SMA will actually perform the atmospheric correction and retrieve the ocean products. In the third phase, it will be applied to wind-blown dust. Our goal is to implement all three phases during FY00. A question that needs to be resolved is whether or not the SMA, which employs a semi-analytic model of ocean color [Gordon *et al.*, "A Semi-Analytic Radiance Model of Ocean Color," *Jour. Geophys. Res.*, **93D**, 10909-10924, 1988], is compatible with more sophisticated ocean color models, e.g., Lee *et al.*, "Method to derive ocean absorption coefficients from remote sensing reflectance," *Applied Optics*, **35**, 453—462, 1996.

The SOA is attractive in that it does not require detailed aerosol models to effect atmospheric correction; however, it is unclear as to its efficacy in dealing with wind-blown desert dust which displays absorption that varies strongly with wavelength. The performance of this algorithm will be studied in parallel with the SMA development.

We have implemented in principle our correction for the polarization sensitivity of MODIS [Gordon, Du, and Zhang, "Atmospheric correction of ocean color sensors: analysis of the effects of residual instrument polarization sensitivity," *Applied Optics*, **36**, 6938-6948]. All that is required now is the analysis of the SBRS polarization characterization measurements by MCST. When these become avaliable, they will be added to the code.

Finally, rather than assuming the sea surface is flat for computing the Rayleigh scattering contribution to the top-of-atmosphere reflectance, we have computed it as a function of wind speed. This addition will improve the performance of the algorithm as described in Gordon, "Atmospheric Correction of Ocean Color Imagery in the Earth Observing System Era," *Jour. Geophys. Res.*, **102D**, 17081-17106, 1997.

3. Study Future Enhancements

There are several enhancements that are now in the research phase. The study of these will continue during FY 2000. The two that we consider most important are (1) developing an accurate model of the subsurface upwelling radiance distribution as a function of view angle, sun angle, and pigment concentration, and (2) evaluating the

performance of the SMA and SOA algorithms in the presence of high concentrations of colored dissolved organic matter (CDOM).

Most validation measurements of upwelled spectral radiance (BRDF) in the water are made viewing in the nadir direction. In contrast, ocean color sensors are usually non-nadir viewing. Thus, an important question is how does one validate the sensor performance when the quantity being measured differs from the quantity being sensed? Obviously, one must either correct the validation measurement to the correct viewing angle of the sensor, or correct the sensor observation to what it would be if the view were nadir. Either strategy requires a model of the subsurface radiance distribution. We are using measurements made near the MOBY site to develop such a model. We started using the model of Morel and Gentili ["Diffuse reflectance of oceanic waters. II. Bidirectional aspects," *Applied Optics*, **32**, 6864—6879 (1993)]; however, that model did not agree well with the experimental results. We are now trying to understand the source of the disagreement by examining processes left out of the computation of the radiance distribution, such as instrument self-shadowing and polarization.

The SMA and the SOA identify the presence of absorbing aerosols by using the full spectrum of radiance at the top of the atmosphere (TOA). Typically, absorbing aerosols cause a depression of the TOA radiance in the blue portion of the spectrum. Unfortunately, CDOM in the water leads to a depression in the blue. We are examining the interference of these two effects. Strong interference could limit the usefulness of ocean color sensors in coastal waters where CDOM is high and absorbing aerosols (from urban pollution) are likely to be present.

Once a model of the BRDF is available, we will use it to correct the diffuse transmittance for BRDF effects as described by Yang and Gordon ["Remote sensing of ocean color: Assessment of the water-leaving radiance bidirectional effects on the atmospheric diffuse transmittance," *Applied Optics*, **36**, 7887-7897 (1997)].

We had originally planned to use MODIS Band 26 (1.38 μm) to correct the imagery for the presence of thin cirrus clouds [Gordon, *et al.*, "Effects of stratospheric aerosols and thin cirrus clouds on atmospheric correction of ocean color imagery: Simulations," *Applied Optics*, **36**, 682-697 (1997)]; however, the modification to the algorithm required to deal with strongly absorbing aerosol appear to be incompatible with our original ideas. For the time being we will use Band 26 only to screen for the presence of thin cirrus.

A difficulty that we have noticed with SeaWiFS imagery is poor performance of the atmospheric correction algorithm at large viewing angles (much larger than will be encountered with MODIS). Presumably this is due to the neglect of the curvature of the earth. We will examine the algorithm to see if the curvature needs to be considered for MODIS.

Validation of MODIS Algorithms and Products

Our participation in validation and initialization exercises requires that an array of instrumentation be maintained and fully operational at all times. Furthermore, data analysis skills need to be maintained as well. Personnel for such maintenance are included in our cost estimates.

4. Participate in MODIS Initialization Campaign

Present plans are to have an initialization field campaign within approximately 90 days of the launch of Terra. We will participate in this campaign by providing several data sets: (1) we shall use our whitecap radiometer [K.D. Moore, K.J. Voss, and H.R. Gordon, "Spectral reflectance of whitecaps: Instrumentation, calibration, and performance in coastal waters," *Jour. Atmos. Ocean. Tech.*, **15**, 496-509 (1998)] to measure the augmented reflectance of the water due to the presence of whitecaps; (2) we shall use our radiance distribution camera system (RADS) to measure the BRDF of the subsurface reflectance; (3) we shall employ our micro pulse lidar (MPL) to measure the vertical distribution of the aerosol (of critical importance when absorbing aerosols are present); (4) we shall use our solar aureole cameras and all-sky radiance camera (SkyRADS) to measure the sky radiance distribution to provide the aerosol scattering phase function; and (5) we will measure the aerosol optical depth (AOD). All measurements will be carried out at the station locations with the exception of the MPL which will operate continuously during the campaign. This data will be combined with the data from MOBY to fine tune the sensor and algorithms.

In addition, we will continue to operate our CIMEL station in the Dry Tortugas as part of the Aeronet Network [Holben, *et al*., "AERONET--A federated instrument network and data archive for aerosol characterization," *Remote Sensing of Environment*, **66**. 1-16]. Data from this site will be used to validate MODIS-derived AOD and possibly provide a means to examine the calibration of the near infrared (NIR) spectral bands.

5. Participate in Validation Campaign (SeaWiFS)

We also plan to participate in the pre-launch validation campaign scheduled for October 1999. This campaign will utilize SeaWiFS imagery to validate the MODIS algorithms and processing software. The measurements what we will make are identical to those described above in reference to the MODIS initialization campaign.

RETRIEVAL OF DETACHED COCCOLITH/CALCITE CONCENTRATION

Algorithm Evaluation/Improvement

We are currently putting effort into evaluating the MODIS coccolith algorithm using historical SeaWiFS observations, converted to synthetic MODIS products. Unfortunately, there have been very few observations of major coccolithophore blooms that were adequately sea-truthed, since the launch of SeaWiFS. The most striking of the features has been the Bering Sea coccolithophore bloom of 1997 and 1998. We enumerated field samples at two sites within the feature, and are comparing these to the derived quantities using the synthetic MODIS product. Our aim over the next year will be to examine other such features that have corresponding sea-truth data. For example, there have been numerous coccolithophore blooms off of the European continental shelf, which were sampled by personnel from the Plymouth Marine Laboratory, (Plymouth, U.K.). We will request coccolith concentration data from these investigators, for comparison with the satellite-derived coccolith concentrations. Moreover, we routinely have been working in the Gulf of Maine, measuring optical properties, enumerating coccolith concentrations, and measuring suspended calcite. These cruises have traversed some relatively coccolith-rich areas (while still considered "non-bloom" they nevertheless should be above the noise threshold of the algorithm).

We have had to change analytical facilities for processing our calcite samples due to non-availability of the previous graphite furnace atomic absorption spectrometer that we were using. We are now working with the Scripps Institution Of Oceanography Analytical Facility, which has an Inductively Coupled Plasma Optical Emission Spectrometer (ICPOES). This instrument is more sensitive than a graphite furnace atomic absorption spectrometer for an equally sized sample. Before they can process our complete set of samples, however, they must first run blanks, and verify proper signal to noise for test samples (happening now). In late September, we will be sending them all unprocessed samples from the Gulf of Maine. Following receipt of the data, we will then collate all data sets that we have for the Gulf of Maine, from 1996 to present, as well as other data that we have collected from the North Atlantic, Caribbean, and Arabian Sea, for revision of the "mean" backscattering versus suspended calcite relationship. This data set would be the largest of its kind available, and the validated relationship will allow significant improvement in the MODIS algorithm code.

Validation of MODIS Algorithms and Products

We are maintaining an active cruise schedule in the Gulf of Maine aboard the ship of opportunity, the passenger ferry m/s *Scotia Prince*. By the end of October, we will have 20 trips for 1999, with 10 more planned for the year 2000. We will make application to continue these trips into upcoming years. These data sets are still being examined, and calcite concentrations are being determined. We also participated in an eight-day cruise to the Gulf of Maine during June and July of this year, aboard the r/v Edwin Linke. These data will be processed over the upcoming months. These trips all have had an above-water radiometer recording upwelling radiance at 40 Deg. from nadir, at the SeaWiFS wavelengths. We will apply the coccolithophore algorithm to these data, for additional validation when satellite coverage is not available. Lastly, we are in the planning stages for a Navy funded experiment to sample the N. Atlantic coccolithophore bloom (ideally this would be during June/July 2001). If funded, this will provide probably the best opportunity for validating the MODIS coccolith algorithm.

MODIS Baseline Spending Plan FY00

The table on the next page delineates the cost to the project on a monthly basis. Travel and shipping have been computed on the following assumptions: (1) we will continue to maintain and operate the AERONET site on the Dry Tortugas at a cost of $600 per month; (2) because of the launch of Terra we have budgeted for four Science Team Meetings (Nov., May, July, Sept.); (3) we plan to send at least one group member to deliver papers at the Fall AGU Meeting, the Ocean Sciences Meeting (Jan.), AGU 2000 (May), and IGARRS 2000 (July); and (4) the MODIS initialization cruise will take place in the March-April time frame. The October cruise costs (travel and shipping) have been included as FY99 costs, i.e., they are reflected in the FY99 carryover. “Communication” included publication page charges. “Maintenance” refers to both hardware and software maintenance of computers. “Subcontracts” refers to the subcontract to Bigelow Laboratory for Ocean Sciences for carrying out the coccolithophore studies. “Capital” refers to procurement of additional mass storage capacity (both increasing the number of disk drives or upgrading low-capacity drives with high-capacity drives) of our Team Member Computer Facility.

Appendix 2

Assessment of Saharan dust absorption in the visible to improve ocean color retrievals and dust radiative forcing estimates from SeaWiFS imagery

Assessment of Saharan dust absorption in the visible to improve ocean color retrievals and dust radiative forcing estimates from SeaWiFS imagery

Cyril Moulin[1,2], Howard R. Gordon[1], Viva F. Banzon[1,3], and Robert H. Evans[3]

[1]Department of Physics, UM, Coral Gables, Florida, USA

[2]Laboratoire des Sciences du Climat et de l'Environnement, CEA-CNRS, 91191 Gif-Sur-Yvette, France

[3]Rosenstiel School of Marine and Atmospheric Science, UM, Miami, Florida, USA

(Submitted to *J. Geophys. Res.*)

Abstract

We have examined forty SeaWiFS images acquired during 1997 and 1998 off the west coast of Africa to develop mineral dust models that could be used for atmospheric correction in this region, i.e., to predict the dust contribution to the measured reflectance in the visible from that measured in the near infrared (NIR). In contrast to most other aerosols, the dust reflectance significantly decreases from the NIR to the blue because of the absorption of mineral particles in the visible. We chose simple, but realistic, vertical structures of the dust layer and examined the applicability of a set of aerosol size distributions and refractive indices with radiative properties computed from Mie theory. We found that eighteen models (six aerosol size-refractive index distributions times three aerosol vertical distributions) were general enough to estimate the dust reflectance in the visible with an absolute RMS error of the order of 5%. We show that these dust models can be used within a "spectral matching algorithm" [*Gordon et al.*, 1997] to effect atmospheric correction of ocean-color imagery in dust-contaminated regions. We also found that our models produce nearly the same top-of-atmosphere out-going visible flux, but that this flux may be significantly different for several other popular dust models. Our computations suggest that this flux is strongly influenced by the absorption and that the use of inappropriate dust models may induce large errors in dust radiative forcing estimates in the solar spectrum.

1. Introduction

Long-range transport of mineral dust in the atmosphere constitutes certainly the most striking feature of the atmospheric aerosol cycle. Indeed, previous works based on series of satellite images over the oceans show that optical depths downwind of arid regions are about an order of magnitude larger than that of typical background conditions [*Moulin et al.* 1997a, *Husar et al.* 1997]. Surprisingly, although desert dust plumes are easy to detect visually on satellite images, the optical properties of these mineral particles still remain poorly know. The most striking and unknown characteristic of mineral dust in the solar spectrum is its ability to absorb in the violet, blue and green portions of the spectrum (350-500 nm). Moreover, this absorption, characterized by the imaginary part of the refractive index of dust particles, is potentially highly variable since it depends on the amount of iron oxides (mainly hematite; see *Sokolik et al.* [1993] and *Claquin et al.* [1999]) in the originating soil.

Thus far, remote sensing of aerosol optical depth from space over the oceans was performed using red and near infrared (NIR) bands. The primary reason is that the marine contribution to the top-of-atmosphere (TOA) radiance is negligible at these wavelengths,. Resulting optical depths have been retrieved within ±20-30% for various sensors by comparison to direct sunphotometer measurements (e.g., *Ignatov et al.* [1995] for AVHRR, *Moulin et al.* [1997b] for Meteosat, *Goloub et al.* [1999] for POLDER). Since most of the aerosols found in the marine environment are composed of pure scattering particles (e.g., sulfates or sea-salts), with almost wavelength-independent optical properties in the visible and NIR, the aerosol optical depth in the red or NIR may be used with confidence to assess the aerosol radiances at other solar wavelengths, and thus to effect atmospheric correction of ocean color or to infer the radiative impact of these aerosols.

The retrieval of ocean chlorophyll concentration, *Chl*, from space (termed "ocean color") is based on the spectral variation of the marine radiance in the blue and green, and relies on the fact that the aerosol radiances in the visible can be accurately computed from the red and NIR radiances, and then removed from the measured radiances to retrieve of the water-leaving radiances. However, as pointed out by *Gordon* [1997], this is not the case when absorbing aerosols are in the atmosphere since the absorption properties of the aerosol (whether weak or strong) are almost impossible to determine by observations in the NIR. Thus all operational atmospheric correction algorithms fail in the presence of absorbing aerosols because, by not being able to assess the aerosol's absorption, they remove too much "aerosol" radiance from the sensor-measured radiance [*Gordon* 1997], and retrieve water-leaving radiances that are too small or even negative. This happens, even if the aerosol's absorption is independent of wavelength, because there will be more atmospheric absorption in the blue than the NIR owing to multiple scattering.

In contrast to the strongly-absorbing aerosols sometimes observed off the U.S. East coast (where the aerosol contains black carbon that absorbs non-selectively with wavelength [*Novakov et al.* 1997, *Russell et al*. 1999]), mineral dust constitutes an extreme case in atmospheric correction because the dust itself is also more strongly

absorbing in the blue than the NIR [*Patterson* 1981]. When atmospheric correction algorithms are applied in the presence of the dust there is a misinterpretation of the too-low derived water-leaving radiance as elevated *Chl*. This is unacceptable because it is believed that dust may supply micro-nutrients to the ocean causing phytoplankton to multiply [*Young et al.* 1991]. Thus, is the enhanced *Chl* real, and due to the presence of dust fertilizing the water, or is it an artifact resulting from a failed atmospheric correction? Similar difficulties occur in the Pacific due to the presence of dust from the Gobi desert [*Fukushima and Toratani* 1997]. In addition, mineral dust covers almost permanently some important oceanic areas all around the world. A prime example is the Tropical Atlantic where dust events occur every two or three days during spring and summer, obscure very productive regions such as the Mauritanian upwelling, and can be often observed all the way to the Americas [*Prospero* 1996, *Husar et al*. 1997].

Two alternative atmospheric correction algorithms have been proposed to deal with strongly-absorbing aerosols: the spectral matching algorithm (SMA) [*Gordon et al.* 1997] and the spectral optimization algorithm (SOA) [*Chomko and Gordon* 1998]. The former uses realistic aerosol models (particle size distribution) with the optical properties of the aerosol (complex refractive index) depending on wavelength, while the latter uses simpler power-law size distributions with wavelength-independent aerosol refractive indices. Both models use a semi-analytic model of ocean color [*Gordon et al.* 1988] to relate the water-leaving radiance to *Chl*. Simulations suggest that both algorithms should perform well in atmospheres with strongly absorbing aerosols, but the SOA algorithm is not applicable in the case of mineral dust, because the dust has a wavelength-dependent absorption. In this paper we focus on the development of dust models (*i.e.*, a particle size distribution and a complex spectral refractive index) that would enable the retrieval of accurate marine chlorophyll concentrations under “dusty” conditions using the SMA.

The lack of knowledge on absorption properties of mineral dust in the visible constitutes the major uncertainty on dust radiative forcing computations, via the spectral single scattering albedo [*Sokolik and Toon* 1996, *Claquin et al*. 1998]. Indeed, because absorption by mineral dust in the visible occurs in the blue and green, where there is still significant input of solar radiation, it has a strong impact on radiative forcing computations when ignored. In addition, *Claquin et al.* [1998] show that the use of a spectrally averaged imaginary part of the refractive index may lead to significant errors on radiative forcing estimates. Since the single scattering albedo is difficult to assess from space [*Kaufman et al.* 1997] and since few in-situ measurements of this imaginary part are available [*Patterson* 1981, *Sokolik et al.* 1993], the more recent radiative forcing models compute on-line the dust absorption properties as a function of the source mineralogy [*Claquin et al.* 1999]. In this framework, dust models suitable for atmospheric of ocean color (i.e., that are capable of representing the radiative effect of dust in the visible) might provide valuable information on the single scattering albedo of mineral dust in the visible, and thus on both TOA outgoing visible flux and dust radiative forcing.

2. Method and data

2.1. Method

The methodology for developing a set of representative models is dictated by the way that the atmospheric correction algorithm is structured. Before discussing the algorithm, we prefer to switch from radiance, L, to reflectance, ρ, where $\rho = \pi L / F_0 \cos\theta_0$. F_0 is the extraterrestrial solar irradiance, and θ_0 is the solar zenith angle. The SeaWiFS atmospheric correction algorithm is structured as follows [*Gordon and Wang* 1994]. After correcting both ozone and water vapor absorption, and estimating the contribution from whitecaps, the remaining spectral reflectance at the sensor for a clear sky pixel can be written

$$\rho_t(\lambda) = \rho_r(\lambda) + \rho_a(\lambda) + \rho_{ra}(\lambda) + t(\lambda)\rho_w(\lambda),$$

where $\rho_r(\lambda)$ is the contribution due to Rayleigh scattering in the atmosphere in the absence of the aerosol, $\rho_a(\lambda)$ is the contribution from scattering by the aerosol in the absence of the air (i.e., Rayleigh scattering), $\rho_{ra}(\lambda)$ is the contribution resulting by interactive scattering between the aerosol and the air, and $\rho_w(\lambda)$ is the contribution from the water-leaving radiance. The quantity $t(\lambda)$ is the diffuse transmittance of the atmosphere, along a path from the sea surface to the sensor, at the wavelength λ. The Rayleigh reflectance $\rho_r(\lambda)$ is accurately computed for each wavelength. The water-leaving reflectance $\rho_w(\lambda)$ is negligible in the NIR (for SeaWiFS, 765 and 865 nm), so in the NIR

$$\rho_t(\lambda) - \rho_r(\lambda) = \rho_a(\lambda) + \rho_{ra}(\lambda) \equiv \rho_A(\lambda)$$

can be determined directly. Given a model for the aerosol, this determination of $\rho_A(\lambda)$ in the NIR uniquely determines $\rho_A(\lambda)$ in the visible. Thus, pragmatically, for the purpose of atmospheric correction we desire a dust model or models that reproduce $\rho_A(\lambda)$ in the visible given $\rho_A(\lambda)$ in the NIR. We could accomplish this by using SeaWiFS in the following manner: given a set of possible aerosol models and SeaWiFS imagery, use the NIR measurements to estimate $\rho_A(\lambda)$ there, compute $\rho_A(\lambda)$ in the visible for each model, and compare the result with the SeaWiFS visible bands. Unfortunately, the only quantity available in the visible is

$$\rho_t(\lambda) - \rho_r(\lambda) = \rho_A(\lambda) + t(\lambda)\rho_w(\lambda),$$

i.e., the only quantity we can determine in the visible, $\rho_A(\lambda) + t(\lambda)\rho_w(\lambda)$, includes the contribution from the water-leaving reflectance. If we knew $\rho_w(\lambda)$, its contribution could be removed because the aerosol model can be used to provide $t(\lambda)$.

2.2. Data selection and processing

We looked at one year (September 1997 — August 1998) of SeaWiFS (sea wide field-of-view sensor) imagery off the coast of Africa to make a list of intense dust events. We selected 40 orbits, listed in Table 1, over the period. Among these, we selected the orbit of June 23, 1998, that displayed the most intense dust transport to satisfy the criterion of high optical depth. High optical depth is desired to reduce the value of $t(\lambda)$, thereby minimizing the influence of the unknown $\rho_w(\lambda)$. We modified the SeaWiFS standard processing code [*Darzi* 1998] to extract $\rho_A(\lambda) + t(\lambda)\rho_w(\lambda)$ for each band and pixel, as well as the complete geometry (θ_0, θ_V and ϕ), where θ_V is the viewing zenith angle and ϕ is the difference of azimuth angle between the viewing and solar directions. SeaWiFS has eight spectral bands (412, 443, 490, 510, 555, 670, 765 and 865 nm). The first change was to cancel the cloud test based on the threshold on the maximum measured radiance at 865 nm. It was necessary because this test was activated for most of the dust plume area, so that corresponding pixels were not processed. The second modification was to replace the standard parameters in the level-2 output file by our set of parameters, which were all already computed at different steps within the standard computer code. We thus used the standard SeaWiFS processing together with ancillary data (wind speed, ozone and water vapor column concentrations) to mask the sun glint, correct ozone and water vapor absorption, and subtract the whitecaps and Rayleigh scattering contributions, forming $\rho_A(\lambda) + t(\lambda)\rho_w(\lambda)$. Plate 1 shows the very high values of this quantity (up to 0.25) within the dust plume. Despite the blind tilt zone and the glitter mask, this dust event seems to originate from the Mauritanian coast and to divide in two branches, one going northward and the other toward the southwest, a characteristic situation for Saharan dust transport during summer [*Karyampudi et al.* 1999].

We extracted both geometry and reflectances from this image along a track across the dust plume, as shown on Plate 1. Because $t(\lambda)$ is expected to be relatively small within this dense dust plume, we have chosen to start our study of existing aerosol models, and the initial development of new dust models, by simply ignoring $t(\lambda)\rho_w(\lambda)$. This limits the study situations in which the aerosol optical is large, e.g., ~1-2. Thus, we removed from the track line data all pixels with $\rho_A(865) < 0.05$. In order to discriminate between clouds and high dust concentration, we applied a threshold on the local variance computed on three consecutive pixels. This is based on the fact that dust plumes are spatially much more homogenous than clouds [*Moulin et al.* 1997b]. We set this threshold by trial and error to 0.01. Extracted reflectances for each band are shown in Figure 1. The major feature of the spectral variation of the measured reflectance is that they strongly decrease in the visible from red to blue. This behaviour is characteristic of absorbing aerosols and is comparable with the computations of *Gordon et al.* [1997] for urban aerosols that contains black carbon. The absorption efficiency of aerosols is reinforced in the blue by means of multiple scattering with air molecules [*Gordon* 1997]. Thus, even for an absorbing aerosol with a spectrally neutral imaginary part of the refractive index, the effect of absorption in the blue is bigger than in the green and red, leading to smaller observed reflectances in the blue.

Although we have tried to minimize the impact of the marine contribution, it is still important to understand the magnitude of the contribution of $t(\lambda)\rho_w(\lambda)$ to the reflectances in Figure 1. The water-leaving reflectance can be written $\rho_w(\lambda) = t_0(\lambda)[\rho_w(\lambda)]_N$, where $[\rho_w(\lambda)]_N$ is the normalized water-leaving reflectance [*Gordon* 1997] and $t_0(\lambda)$ is the diffuse transmittance of the atmosphere along a path from the sun to the sea surface [*Yang and Gordon* 1997]. Values of $[\rho_w(\lambda)]_N$ are provided in Table 2 for clear ocean water (low *Chl*). These were computed using the semi-analytic model of ocean color developed by *Gordon et al.* [1988], and a *Chl* concentration of 0.05 mg/m^3. The values of the diffuse transmittances used to estimate $t(\lambda)\rho_w(\lambda)$ were taken from a classical dust model (BDS1; described in Section 3.1 below) with aerosol optical depths at 865 nm, $\tau_a(865)$ of 1.0 and 1.8, and the geometry of the track shown in Plate 1. The values of $t(\lambda)\rho_w(\lambda)$ at 412, 443, 490, and 510 nm in the table are conservative in that if *Chl* is higher the values of $[\rho_w(\lambda)]_N$ are lower, while at 555 nm, it is possible for the reflectance to be ~ 50% higher than provided in Table 2. In Figure 1, the marine contribution may thus account for about 10 to 20% of the measured reflectances at 412 and 443 nm, for about 5 to 10% at 490 and 510 nm, and for less than 5% in other visible bands. This confirms that the observed spectral behaviour of the reflectance is primarily driven by the dust optical properties, and that our hypothesis of negligible marine contributions is valid to first order.

It is also very important to understand how SeaWiFS is sensitive to the very high reflectances in Figure 1. SeaWIFS was designed specifically for studying the dynamics of the primary productivity of the oceans on a global scale. It has the required high radiometric sensitivity for retrieving the water-leaving reflectance in the visible portion of the spectrum as well as spectral bands in the NIR for atmospheric correction. One unique feature is a bilinear radiometric response so there is high sensitivity for dark targets and low sensitivity for bright targets. This is achieved with a 10-bit digitization. The transition from high to low sensitivity takes place around 760 digital counts (DC), referred to as the "knee" in the gain curve [*Hooker et al.* 1992, *Barnes et al.* 1994]. Along the track shown in Figure 1, the radiance in the NIR is always in the upper (less sensitive) part of the gain curve. In contrast, the blue bands (412, 443, and 490 nm) are almost always in the lower (more sensitive) part of the gain curve. For the rest of the spectral bands, the lower reflectance are in the lower part of the gain curve but not the higher values. This shows that no band reaches the saturation value for this very dense dust plume, and that the blue and blue-green channels rarely reach the calibration knee, above which the accuracy of the measurement is reduced.

A remarkable feature in Figure 1 is seen between 23°N and 26°N. This corresponds to the most intense part of the dust plume (just west of Cabo Barbas, Western Sahara). In this region the reflectance in the NIR increases rapidly from about 0.1 to 0.23. In stark contrast, the reflectance at 412 nm remains almost constant at about 0.05. For the other bands, the reflectance increasingly increases proceeding from the blue to the red. It appears that the blue reflectance essentially saturates in the sense that the reflectance becomes almost independent of the aerosol optical depth

(or the aerosol concentration). Table 2 suggests that this cannot be due to variations in the water properties.

The 23°N-26°N region is contrasted with the region from 15°N and 16°N, where the NIR increases from about 0.1 to 0.15. In this case, all of the spectral bands follow the increase in the visible, although the variation is smaller at 412 nm than at 865 nm. Another interesting observation is that for some regions, the reflectance at 670 nm is larger than that at 865 nm, while in other regions it is lower. Further interpretation of these results at this point is hampered by that fact that $t(\lambda)\rho_w(\lambda)$ is included in the reflectance, but is not precisely known. The results, however, do suggest that some property of the aerosol, other than its concentration is varying over the track line. Possible candidates for the variability are the particle size distribution which may vary during transport, the refractive index which depends on the location of the dust source, and the vertical distribution which changes with meteorological conditions.

3. Determination of appropriate absorbing dust models

3.1. Selection of a baseline model for Saharan dust

A so-called "dust model" consists of a size distribution that provides particle radius, and a complex refractive index that enables definition of the optical properties of the aerosol using Mie theory. It is generally accepted that aerosol size may be represented by one, or a combination of two or three, lognormal distributions [*D'Almeida et al.* 1991], each lognormal mode being defined by a mean radius and a standard deviation. *Moulin et al.* [1997c] reviewed various mineral dust models with one to three modes, and showed that the corresponding optical properties may be completely different from one model to the other. This is particularly important for remote sensing applications, since the size distribution of mineral dust is believed to dramatically change during the transport because of the size dependency of the particle settling velocity (i.e., large particles have a shorter residence time in the atmosphere). The complex refractive index of aerosols depends on its chemical composition: the real part n_R characterizes the scattering properties of the medium, while the imaginary part n_I characterizes the absorption properties of the material. As discussed by *Moulin et al.* [1997c] very few measurements of mineral dust refractive index are available. There is however a general agreement on a mean value of 1.50-1.55 for n_R, spectrally neutral in the visible. The imaginary part of mineral dust is more poorly known, although it is generally recognize that n_I is relatively small in the red and NIR, and that it sharply increases from green to blue because of the absorption by iron oxides such as hematite [*Sokolik et al.* 1993]. *Patterson* [1981] published the only available review on measurements of the imaginary part of the refractive index of Saharan dust and showed that n_I varies from 0.025 at 0.3 μm to 0.004 at 0.7 μm.

We used radiative transfer simulations to compute $\rho_A(\lambda)$ from $\rho_A(865)$ at each pixel along the track line in Figure 1**,** for several dust models. The atmospheric radiative transfer model was a two-layer atmosphere bounded by a flat fresnel-reflecting sea surface [*Gordon and Wang* 1994]. We then compared the extracted

values of $\rho_A(\lambda) + t(\lambda)\rho_w(\lambda)$ with predictions of $\rho_A(\lambda)$. We tested the different size distributions described by *Moulin et al.* [1997c] as well as the "long-range transport mineral dust" model of *D'Almeida et al.* [1991], hereafter referred as MIS. For all of them, we used $n_R = 1.53$ and the values of n_I given by *Patterson* [1981]. Figure 2 provides examples of the simulated reflectance spectrum for the most representative dust models. The Background Dust model of *Shettle* [1984], hereafter referred as BDS1, has three modes that cover a wide range of particle radius and was found to be the most suitable size distribution to retrieve African dust optical depths from Meteosat imagery [*Moulin et al.* 1997c]. The D5S model has a single mode and is representative for "Dust at 5000 km" [*Schütz* 1979] that was also used for comparison by *Moulin et al.* [1997c]. The MIS model has a single mode and is often used as characteristic of mineral dust for remote sensing studies [e.g., *Antoine and Morel* 1998]. For comparison, we also ran the radiative transfer model on the "Maritime model at 90% relative humidity" (M90) of *Shettle and Fenn* [1979] used for testing the standard SeaWiFS atmospheric correction [*Gordon and Wang* 1994]. This model is provided as an example of a non-absorbing aerosol which is typical of an open ocean environment free of terrigenous and anthropogenic influences. Comparison of Figures 1 and 2 show that BDS1 is the only model which fits correctly the SeaWiFS reflectances for the track line. Note that this is true over the whole set of tested models, not only among the three models displayed on Figure 2. The D5S and mostly the MIS models obviously have far too much absorption despite the fact that they have the same refractive index than the BDS1 model. This difference is thus due to their size distribution that certainly does not fit the actual dust size distribution. Note that the "Dust at 2000 km" [*Schütz* 1979] that was also described in Moulin et al. [1997c] leads to a worst result than the MIS model in Figure 2, mainly because its size distribution includes a lot of very large particles. In contrast, the M90 model leads to spectrally neutral reflectance and cannot reproduce the spectral variation. This illustrates the fact that the standard SeaWiFS atmospheric correction fails for absorbing aerosols: the measured reflectances in the blue and the green are corrected using aerosol reflectances that are too large. This leads to too small or even to negative water-leaving reflectances. We concluded from this comparison that the BDS1 size distribution associated with a refractive index defined by $n_R = 1.53$ and the *Patterson* [1981] spectral n_I constitutes a reasonable baseline dust model to study the Saharan dust absorption properties in the visible.

3.2. Expected variability of Saharan dust reflectances

Thickness of the dust layer. *Gordon* [1997] has shown that the aerosol vertical structure is an important consideration in the reflectance of the ocean-atmosphere system in the presence of strongly absorbing aerosols. Indeed, absorption efficiency of aerosols tends to be higher when particules are mixed with air molecules in a thicker layer because the multiple scattering effect increases. We thus set up the radiative transfer model to enable different mixing heights. As shown on Figure 3, several vertical structures were tested for the dust layer: v00 in which the aerosols are all confined in the lower layer with all of the molecular (Rayleigh) scattering is confined to the upper layer; v02 (respectively v04, v06 and v08) in which the aerosols

are uniformly mixed with air from the surface to 2 km (respectively 4, 6 and 8 km); vUU in which the aerosols are uniformly mixed with air throughout the atmosphere. The v00 vertical structure, which leads to the smallest absorption efficiency, is usually used to compute the non-absorbing aerosol reflectance and was used also for the model comparison in Figure 2. Figure 3 clearly shows that the vertical structure of the dust layer has a strong impact on $\rho_A(\lambda)$ in the blue and that this effect becomes small for wavelengths greater than 500 nm. Noting that the water contribution is included in the measured values of $\rho_A(\lambda)$ in Figures 3a and 3b, the data points will all move to lower values (0.01 to 0.006 at 412 nm and 0.008 to 0.005 at 490 nm, see Table 2), it is clear that the BDS1 model cannot fit the SeaWiFS data for data between 23°N and 26°N (the "flat" part of the $\rho_A(412)$ versus $\rho_A(865)$ relationship) at both 412 and 490 nm unless the aerosol is well mixed throughout the atmosphere. As the dust rarely reaches an altitude greater than 5-6 km [*Prospero and Carlson* 1972], this implies that the BDS1 model has too little absorption to fit all the measured reflectances. On the contrary, for the other data (the "linear" part of the $\rho_A(412)$ versus $\rho_A(865)$ relationship), the BDS1 model appears to have too much absorption. Indeed, simulations are slightly too low at 412 nm, and are much too low at 490 nm, to fit the data.

Size distribution. As it is clear that the BDS1 model is not appropriate for the "flat" portion of the $\rho_A(412)$ versus $\rho_A(865)$ relationship (see Figure 3a) because of a lack of absorption, a modification was necessary. The simplest change was to increase the fraction of large particles relative to small. This is not unreasonable since that portion of the track, as shown on Plate 1, visually appears to be the closest to the coast, and thus to the source, so that large particles would be more numerous. To do so, we simply increased the relative contribution in number of the large mode by factors of 10 and 20 forming what we called respectively the BDS2 and BDS3 models. It is important to note, as discussed by *Moulin et al.* [1997c], that such an increase of the large mode contribution may not be realistic in term of mass computation. Figure 4 compares the reflectances computed using the BDS3 model with the extracted data at both 412 and 490 nm. On Figure 4a, it is clear that the "flat" portion of the relationship at 412 nm can be explained by the BDS3 model well-mixed to an altitude between 2 and 4 km, suggesting that it is possible to explain the data at 412 nm using the BDS1 model by varying the vertical distribution and the relative abundance of large particles. Figure 4b leads to the same conclusion for the "flat" part of the data at 490 nm, even if the absorption of the BDS3 model may be slightly too high. However, the too high absorption for the "linear" part of the $\rho_A(412)$ versus $\rho_A(865)$ shown on Figure 3 obviously worsen with these increases of the large mode contribution. To compensate this, we tried to create BDS models with less large particles to decrease the absorption, but it turned out that, as discussed by *Moulin et al.* [1997b], the optical contribution of the large mode to the BDS1 model is so small that it can be removed without any effect. We thus concluded that for these "linear" portion of the data, the $\rho_A(\lambda) + t(\lambda)\rho_w(\lambda)$ versus $\rho_A(865)$ relationships cannot be all explained by the BDS models.

Imaginary part of the refractive index. The second method available for reducing the absorption for a given model is to reduce the imaginary part of its

refractive index, n_I. Such a decrease in the absorption efficiency of dust is not unrealistic since n_I is directly related to the amount of hematite in the dust particles. Indeed, *Claquin et al.* [1999] recently showed that the dust uplifted in the Sahara contains significantly less hematite, and is thus much less absorbing, than the dust coming from the Sahelian region. It is thus possible that the *Patterson's* [1981] imaginary part corresponds to a relatively high content of hematite. Reduction of n_i was carried out by trial-and-error for all of the bands to achieve a reasonable fit to the extracted data. We thus defined a new set of dust models, the "Background Dust of this Work" (BDW) models which have the same size distributions as the BDS models, but lower imaginary part of the refractive index. The spectral variation of n_I for both BDS and BDW models are given in Table 3. Figure 5 shows the result of the comparison between measured and computed reflectances for the BDW models at 490 nm. It is clear that the BDW models can fit the 490 nm extractions reasonably well. It is important to note that since there is still some water contamination in the extractions, the value of n_I resulting from this procedure are *minimum* values for the given size distributions. Thus, the n_I's for the BDW models may be slightly too small in the blue and the green, but that is acceptable for this work because the n_I's for the BDS distributions are likely to be slightly too large.

3.3. Summary of the final set of dust models

The result of these exercises is two dust models — the original BDS and the new BDW — for each of which we can vary the thickness of the aerosol layer as well as the fraction of large particles in the size distribution. In order to restrict the number of combinations and to be coherent with both winter and summer observed transport patterns, we limited the possibilities to three different dust layer thickness, i.e., 2, 4 and 6 km [*Chiapello et al.* 1995; *Karyampudi et al.* 1999; *Prospero and Carlson* 1972]. We thus ended up with 18 combinations resulting from 2 spectra of the imaginary part of the refractive index, 3 size distributions, and 3 vertical structures of the dust layer. The spectral behavior of the single scattering albedo, ω_0, for each model is provided in Figure 6. In the following section, we perform a statistical analysis of several dust plumes to verify that these models are capable to represent the observed spectral dust reflectances of most situations encountered off the African coast.

4. Application to atmospheric correction of ocean color

To test the wider applicability of these dust models for atmospheric correction, we extracted reflectances (i.e., $\rho_A(\lambda) + t(\lambda)\rho_w(\lambda)$) along the same track as in Plate 1 for the whole set of images described in Table 1. Because the criterion of very high optical depth was not respected for all of the dust plumes, as it was for the one displayed in Plate 1, it was not possible to systematically neglect the marine contribution when comparing measured and computed reflectances in the blue. We thus set up a procedure to read the CZCS climatological monthly-mean *Chl* associated with each pixel along each track. This *Chl* enabled an estimate of the water-leaving reflectance $[\rho_w(\lambda)]_N$ to be obtained. Then, for each aerosol model (size distribution,

refractive index, and vertical distribution) we used $\rho_A(865)$ to estimate the aerosol optical depth at 865 nm, and from this computed the diffuse transmittances, $t(\lambda)$, along the track. In this manner, we are able to estimate $\rho_w(\lambda)$ for a given model, and thus to obtain a better approximation to the "observed" $\rho_A(\lambda)$ from the measured reflectances. We then computed the mean RMS difference over all bands between the "observed" values of $\rho_A(\lambda)$ and those computed for the particular model using the method described in the previous section. Carrying out this procedure for all of the 18 models we selected the best model as that with the lowest RMS differences for between the observations and the model predictions. Note that all models fit perfectly at 865 nm at each pixel, since this band is used as an "anchor point" to compute the optical depth, so that the RMS residual is actually computed on bands 412 to 765 nm.

The results of this selection process applied to the 40 tracks of 400 pixels each (~3700 pixels processed after cloudy and "non-dusty" pixel removal) are summarized in Figure 7, which provides the histogram of the RMS error in the fit. Because we have used monthly means for *Chl* to estimate the water contribution, $t(\lambda)\rho_w(\lambda)$, we also estimated the contribution using half and double the monthly mean values of *Chl*. The frequency distribution of the residual error (in %) for the individual pixels are provided in Figure 7 for each estimate of *Chl*. We note that the errors are typically between 3 and 6 %, and that the value used for the pigment concentration is not important. Approximately 90% of the residuals are less than 6 %. Higher residuals are mostly related to very high aerosol optical depths (e.g., those along the "flat" portion of the $\rho_A(\lambda) + t(\lambda)\rho_w(\lambda)$ versus $\rho_A(865)$ relationship in Figure 3). For the whole data set, we also computed histograms of the error in $\rho_A(\lambda)$ for individual bands throughout the visible. The histograms were generally "gaussian shaped" with a full width at half maximum of about 0.005. The position of the histogram maximum for each SeaWIFS band is provided in Table 4. This shows that the absolute error on $\rho_A(\lambda)$ is most of the time lower than 0.002 in the blue and in the green, even for high optical depth. Such an accuracy meets the typical requirements for atmospheric correction of ocean color imagery (i.e., 0.002 on $\rho_A(\lambda)$, [*Gordon* 1997]).

The distribution of models that minimize the residuals at each pixel are provided in Figure 8. The relationship between the model number and model code is provided in Table 5. It is interesting to note that the model chosen is often that with the aerosol distributed from the surface to 6 km, i.e., 6, 12, 15, and 18. This suggests that for the spectral variation of the absorption index that we have used, the way to achieve the correct spectral variation of $\rho_A(\lambda)$ is to mix the aerosol high into the atmosphere. The fraction of pixels for which these models were chosen was 50.9, 41.6, and 61.7% for the CZCS monthly mean *Chl*, double the monthly mean, and half the monthly mean, respectively. The variation of the chosen model with the pigment estimate is easy to understand. Generally the BDW models have less absorption than the BDS models. Also, for a given model the reflectance in the blue decreases as the aerosol is mixed higher into the atmosphere (Figure 3a). With increasing pigments, $t(\lambda)\rho_w(\lambda)$ in the blue decreases compared to the green. Thus when the pigments increase, there is a smaller water contribution to $\rho_A(\lambda) + t(\lambda)\rho_w(\lambda)$, so $\rho_A(\lambda)$ will be larger, requiring a model with less absorption. Thus, the "double *Chl*" model choices will move to those with lower absorption, while the "half *Chl*" choices are toward

higher absorption. This is particularly important for ocean color since it shows that our procedure is capable of adapting to a change in chlorophyll concentration by switching from one model to the other (Figure 8), but by keeping the same accuracy (Figure 7). These results suggest that our dust models provide optical properties in the visible that are representative of most of the absorbing mineral dust transported over the Tropical Atlantic off the African coast, and that they offer the required accuracy to be used within the "spectral matching algorithm" of *Gordon et al.* [1997] to derive the marine chlorophyll concentrations in dust-contaminated regions.

5. Application to radiative forcing estimate

We have seen that these models were capable of representing accurately the spectral behaviour of the "observed" aerosol reflectances for most of the dust transport situations and for a wide range of geometry (θ_0, θ_V and ϕ), and thus of scattering angle, throughout the year. It is of interest to understand the direct radiative forcing predicted by these models. The procedure described in the previous section uses a climatological value of *Chl* to estimate the water-leaving reflectance and select the dust model that leads to the best agreement between the "observed" and retrieved aerosol reflectances. Given this dust model and $\rho_A(865)$, it is straightforward to compute, within the radiative transfer model, the instantaneous outgoing flux at the top-of-atmosphere (TOA) as well as the flux absorbed in the atmosphere and in the ocean in each of the SeaWiFS spectral bands. It will be a simple matter to produce LUTs in which the TOA outgoing flux $E\uparrow(\lambda)/F_0(\lambda)$, where $E\uparrow(\lambda)$ is the outgoing flux, is provided as a function of $\rho_A(865)$ for each aerosol model, enabling retrieval of the instantaneous outgoing flux. This flux could then be used to estimate the instantaneous radiative forcing of Dust (*IRFD*) over the SeaWiFS spectral range (0.4 to 0.9 μm) due to the presence of the dust:

$$IRFD(\theta_0) = \int_{0.4}^{0.9} E\uparrow(\lambda,\theta_0)d\lambda - \int_{0.4}^{0.9} E_r\uparrow(\lambda,\theta_0)d\lambda \ ,$$

where $E_r\uparrow(\lambda,\theta_0)$ is the outgoing flux in the absence of the aerosol at the solar zenith angle (θ_0) at the time of the satellite overpass. Note, that with this definition, a positive $IRFD(\theta_0)$ indicates that the aerosol causes more energy to escape to space, *cooling* the planet. Figure 9 provides an example of the *IRFD* for the aerosol models studied in this work, for geometry similar to the track on Plate 1. In preparing Figure 9 we bisected the wavelength interval between each set of adjacent bands and, for a given spectral band, averaged the extraterrestrial solar irradiance over the interval containing the band, e.g., for the band at 510 nm, $F_0(510)$ was the average of $F_0(\lambda)$ over the interval 500 to 532.5 nm. The value of $E\uparrow(\lambda,\theta_0)$ was taken to be constant in each interval. Also, the presence of absorption bands due to water vapor and ozone was ignored. Two additional models are included on Figure 9: D5S [*Schütz* 1980] and BDC, the BDS-BDW size distributions but with a constant $n_I = 0.0005$ (same as

BDW at 865 nm) throughout the spectrum. The BDC's represent the limit of a weakly-absorbing aerosol with the same size distributions as BDS and BDW.

A striking feature of the results presented in Figure 9 is the wide range of values for $IRFD(\theta_0)$ over the various models. Considering all of the models in Figure 9, the full range of values of the $IRFD(\theta_0)$ varies by over a factor of 2 for a given $\rho_A(865)$ (almost 3 at $\rho_A(865) = 0.2$), but the variation is significantly less, about 20%, when considering the BDS and BDW models only (~95 to 118 W/m^2 at $\rho_A(865) = 0.2$). This suggest that the $IRFD(\theta_0)$ associated to a given $\rho_A(865)$ has a slight but not negligible dependency on which of our eighteen dust models has been chosen by the procedure. It is also important to note that for an individual dust model, the vertical structure can also make a significant impact on $IRFD(\theta_0)$, e.g., for BDS1 near $\rho_A(865) = 0.2$ the v00 and vUU yield ~110 and 100 W/m^2, respectively. On the contrary, Figure 9 shows that the use of not suitable models, such as D5S or MIS, significantly reduces the retrieved $IRFD(\theta_0)$ (by up to a factor of 2) because of their to high absorption (see section 3.1). The comparison between the $IRFD(\theta_0)$ computed for the BDS-BDB models and the BDC models (weakly absorbing) shows that the dust absorption in the blue reduces the outgoing flux by 10 to 30%. This result clearly shows that the absorption in the blue and the green has a significant impact on the computation of the dust radiative forcing in the solar spectrum, and that the use of wrong models may lead to large errors. We thus believe that this outgoing flux computation could be done within the "spectral matching algorithm" of *Gordon et al.* [1997] by using the retrieved *Chl* and dust model. If we are willing to accept that the state of the aerosol at the time of measurement remains relatively constant through out the day at the given location, then the mean radiative forcing for the entire day can be computed as well. Furthermore, the individual aerosol models could be extended to larger wavelengths allowing evaluation of the mean short-wave radiative forcing.

6. Conclusions

We have examined SeaWiFS images acquired during 1997 and 1998 off the west-coast of Africa, where the atmosphere frequently contains large quantities of desert dust from both the Sahara and the Sahel. The methodology we used, developing models that reproduce the observed SeaWiFS $\rho_A(\lambda) + t(\lambda)\rho_w(\lambda)$ versus $\rho_A(865)$ relationship, was dictated by our desire to develop dust models that could be used for atmospheric correction of SeaWiFS imagery in this region, i.e., to predict the aerosol contribution to the reflectance in the visible from that measured in the NIR.

We found that, of several popular models proposed in the literature, only the models with the size distribution similar to that proposed by *Shettle* [1984] and the refractive index (real and imaginary parts) determined from measurements of dust samples [*Patterson*, 1981] provided the correct spectral variation of the aerosol contribution to the reflectance. Our results also demonstrate that the vertical distribution of the aerosol is as important as the absorption index in establishing the $\rho_A(\lambda) + t(\lambda)\rho_w(\lambda)$ versus $\rho_A(865)$ relationship. We refined this model by introducing two modifications: we increased the relative concentration in Shettle's large particle mode; and decreased somewhat Patterson's absorption index.

After accounting for the water's contribution using a realistic value of *Chl* to compute the water-leaving reflectances, it was found that the resulting eighteen models (six aerosol size-refractive index distributions times three aerosol vertical distributions) were general enough so that, for the 40 images examined, ρ_A in the visible could be estimated from ρ_A in the NIR (865 nm) with an RMS error of the order of 5%. For the 40 images, the absolute RMS error was ~0.001 to 0.002 at most wavelengths, which is sufficient for atmospheric correction of ocean color. Since we also showed that this accuracy does not change when the *Chl* value varies, but that an other dust model is picked up, we believe that our set of mineral dust models could be successfully used within the "spectral matching algorithm" of *Gordon et al.* [1997] to derive the marine chlorophyll concentration in dust-contaminated regions. Another important conclusion of this part of the work is that Saharan dust does not show a wide range of optical properties in this region of the Atlantic Ocean (see **Plate 1**) and that it is possible to accurately represent its absorption with only two refractive indices. It would be interesting to try to correlate each index to different source regions and to see how the mineralogy of soils [*Claquin et al.* 1999] influences the imaginary part of the dust aerosol refractive index.

Since our dust models turned out to be in very good agreement with SeawiFS spectral measurements, we explored their potential for aerosol radiative impact studies. We found that our eighteen models produce nearly the same TOA outgoing flux (within ±10%), but that the out-going flux is significantly larger than for the rejected models. We also showed that the mineral dust absorption in the visible may have a large impact on the instantaneous radiative forcing of dut in the solar spectrum and has to be carefully taken into account. The recent launch of the Terra satellite with the sensor MODIS provides the possibility of better defining the optical properties of mineral dust particles by using new spectral bands in the infrared. We believe that these dust models are capable of providing a good estimate of the instantaneous TOA outgoing flux estimated directly from $\rho_A(865)$, which is nearly independent of the aerosol vertical structure, using the "spectral matching algorithm" to provide the "best" dust model.

Acknowledgment

The authors are grateful for support for this work under the following grants and contracts: NASA NAS5-31363 (HRG, CM), NASA NAS5-31734 (HRG, VFB), NASA NAS5-31XXX (RHE). Additional support was provided by the French Commissariat à l'Energie Atomique (CEA) and Centre National de la Recherche Scientifique (CNRS). This is contribution XXX from LSCE.

References

Antoine, D. and A. Morel, An algorithm for detection of desert dust from TOA ocean color spectra (MERIS instrument): Demonstration using SeaWiFS data, *Ocean Optics XIV,* Kailua-Kona Hawaii, November 10-13, 1998.

Barnes, R.A., A.W. Holmes, W.L. Barnes, W.E. Esaias, C.R. McClain, and T. Svitek, SeaWiFS prelaunch radiometric calibration and spectral characterization,

SeaWiFS Technical Report Series: Volume 23, NASA Technical Memorandum 104566, Eds. S.B. Hooker, E.R. Firestone, and J.G. Acker, Greenbelt, MD, October 1994.

Chiapello, I., G. Bergametti., L. Gomes, B. Chatenet, F. Dulac, J. Pimenta, E. Santos Suares, An additional low layer transport of Sahelian and Saharan dust over the North-Eastern Tropical Atlantic, *Geophys. Res. Lett.*, 22, 3191-3194, 1995.

Chomko, R. and H.R. Gordon, Atmospheric correction of ocean color imagery: Use of the Junge power-law aerosol size distribution with variable refractive index to handle aerosol absorption, *Applied Optics* **37**, 5560—5572, 1998.

Claquin, T., M. Schulz, Y. B. Balkanski, and O. Boucher, Uncertainties in assessing radiative forcing by mineral dust, *Tellus*, 50B, 491-505, 1998.

Claquin, T., M. Schulz, and Y.J. Balkanski, Modeling the mineralogy of atmospheric dust sources, *J. Geophys. Res*., 104, 22243 22256, 1999.

D Almeida, G.A., P. Koepke, and E.P. Shettle, Atmospheric Aerosols, Global Climatology and Radiative Characteristics, A. Deepak, Hampton, VA, 1991, pp. 561.

Fukushima, F. and M. Toratani, Asian dust aerosol: Optical effect on satellite ocean color signal and a scheme for its correction, *J. Geophys. Res.*, 102D, 17119—17130, 1997.

Darzi, M., SeaWIFS Science Algorithm Flow Chart, NASA/CR-1988-206848 NASA/GSFC Greenbelt, MD, 1998.

Goloub, P., D. Tanr , J. L. Deuz , M. Herman, A. Marchand, and F. M. Br on, Validation of the first algorithm applied for deriving the aerosol properties over the ocean using the POLDER/ADEOS measurements, *IEEE Trans. Geosci. Remote Sensing*, 37, 1586-1596, 1999.

Gordon, H.R., O.B. Brown, R.E. Evans, J.W. Brown, R.C. Smith, K.S. Baker, and D.K. Clark, A Semi-Analytic Radiance Model of Ocean Color, *Jour. Geophys. Res.*, 93D, 10909—10924, 1988.

Gordon, H.R. and M. Wang, Retrieval of water-leaving radiance and aerosol optical thickness over the oceans with SeaWiFS: A preliminary algorithm, *Applied Optics*, **33**, 443—452, 1994.

Gordon, H.R., Atmospheric Correction of Ocean Color Imagery in the Earth Observing System Era, *Jour. Geophys. Res.*, 102D, 17081—17106, 1997.

Gordon, H.R, T. Du, and T. Zhang, Remote sensing ocean color and aerosol properties: resolving the issue of aerosol absorption, *Applied Optics*, **36**, 8670—8684, 1997.

Hooker, S.B., W.E. Esaias, G.C. Feldman, W.W. Gregg, C.R. McClain, An Overview of SeaWiFS and Ocean Color, *SeaWiFS Technical Report Series: Volume 1*, NASA Technical Memorandum 104566, Eds. S.B. Hooker and E.R. Firestone, Greenbelt, MD, July 1992.

Husar, R.B., L.L. Stowe, and J.M. Prospero, Characterization of tropospheric aerosols over the oceans with the NOAA advanced very high resolution radiometer optical thickness operational product, *Jour. Geophys. Res.*, 102D, 16889 16909, 1997.

Ignatov, A. M., L. L. Stowe, S. M. Sakerin, and G. K. Korotaev, Validation of the NOAA/NESDIS satellite aerosol product over the North Atlantic in 1989, *J. Geophys. Res.*, 100, 5123-5132, 1995.

Karyampudi, V.M., S.P. Palm, J.A. Reagen, H. Fang, W.B. Grant, R.M. Hoff, C. Moulin, H.F. Pierce, O. Torres, E.V. Browell and S.H. Melfi, Validation of the Saharan dust plume conceptual model using lidar, Meteosat and ECMWF data, *Bull. Amer. Meteorol. Soc.*, vol. 80, no. 6, 1045-1075, 1999.

Kaufman, Y. J., D. Tanré, H.R. Gordon, T. Nakajima, J. Lenoble, R. Frouin, H. Grassl, B.M. Herman, M.D. King and P.M. Teillet, Passive remote sensing of tropospheric aerosol and atmospheric correction for the aerosol effect. *J. Geophys. Res.* 102, 16815–16830, 1997.

Moulin, C., C.E. Lambert, F. Dulac, and U. Dayan, Control of atmospheric export of dust from North Africa by the North Atlantic Oscillation, *Nature*, *387*, 691-694, 1997a.

Moulin, C., F. Guillard, F. Dulac, and C.E. Lambert, Long-term daily monitoring of Saharan dust load over ocean using Meteosat ISCCP-B2 data, 1, Methodology and preliminary results for 1983-1994 in the Mediterranean, *J. Geophys. Res.*, 102, 16,947-16,958, 1997b.

Moulin, C., F. Dulac, C.E. Lambert, P. Chazette, I. Jankowiak , B. Chatenet, and F. Lavenu, Long-term daily monitoring of Saharan dust load over ocean using Meteosat ISCCP-B2 data, 2, Accuracy of the method and validation using sunphotometer measurements., *J. Geophys. Res.*, *102*, 16,959-16,969, 1997c.

Novakov, T., D.A. Hegg, and P.V. Hobbs, Airborne measurements of carbonaceous aerosols on the East Coast of the United States, *Jour. Geophys. Res.*, 102D, 30023 30030, 1997.

Patterson, E.M., Optical Properties of Crustal Aerosol: Relation to Chemical and Physical Characteristics, *J. Geophys. Res.,* 86C, 3236 3246, 1981.

Prospero, J. M. and T. N. Carlson, Vertical and areal distribution of Saharan dust over the western equatorial North Atlantic Ocean, *J. Geophys. Res.*, 77, 5255-5265, 1972.

Prospero, J.M., The atmospheric transport of particles to the ocean, in Particle Flux in the Ocean, *edited by P. Schäfer et al.*, pp. 19-52, John Wiley, New York, 1996.

Russell, P. D., P. V. Hobbs, and L. L. Stowe, Aerosol properties and radiative effects in the United States East Coast haze plume: An overview of theTropospheric Aerosol Radiative Forcing Operational Experiment (TARFOX), *Jour. Geophys. Res.*, 102D, 2213 2222, 1999.

Shettle, E. P. and R. W. Fenn, Models for the Aerosols of the Lower Atmosphere and the Effects of Humidity Variations on Their Optical Properties, *AFGL--TR--79-0214*, Air Force Geophysics Laboratory, Hanscomb AFB, MA, 1979.

Shettle, E. P. (1984) Optical and radiative properties of a desert aerosol model, In *Proc. Symposium on Radiation in the Atmosphere*, ed. G. Fiocco, Hampton, Va.: A. Deepak.

Schütz, L., Long range transport of desert dust with emphasis on the Sahara, *Ann. N.Y. Acad. Sci.*, 338, 15-20, 1980.

Sokolik, I. N., A. Andronova, and T. C. Johnson, Complex refractive index of atmospheric dust aerosols, *Atmos. Env.*, 27A, 2495-2502, 1993.

Sokolik, I. N. and O. B. Toon, Direct radiative forcing by anthropogenic airborne mineral aerosols, *Nature*, 381, 681-683, 1996.

Young, R.W., K.L. Carder, , P.R. Betzer, D.K. Costello, R.A. Duce, G.R. Ditullio, N.W. Tindale, E.A. Laws, M. Uematsu, J.T. Merrill, and R.A. Feeley, Atmospheric Iron Inputs and Primary Productivity: Phytoplankton Responses in the North Pacific, *Global Biogeochemical Cycles*, 5, 119 134, 1991.

Yang, H. and H.R. Gordon, Remote sensing of ocean color: Assessment of the water-leaving radiance bidirectional effects on the atmospheric diffuse transmittance, *Applied Optics*, **36**, 7887—7897, 1997.

Tables

Table 1. Selected SeaWiFS images of dust plumes off the coast of Africa and number of "dusty" pixels among the 400 pixels of the track shown in Figure 1.

Day	Number of "dusty" pixels
9/22/97	17
10/3/97	86
10/5/97	69
11/5/97	2
12/26/97	42
12/28/97	118
1/6/98	86
1/8/98	99
1/10/98	43
1/15/98	73
1/17/98	59
2/6/98	11
2/15/98	224
2/17/98	35
2/23/98	118
2/25/98	150
2/26/98	164
2/27/98	156
2/28/98	74
3/6/98	163
3/8/98	223
3/9/98	167
3/10/98	133
3/11/98	103
3/22/98	149
3/31/98	110
5/11/98	79
5/12/98	76
5/31/98	69
6/2/98	37
6/3/98	40
6/20/98	49
6/22/98	121
6/23/98	116
6/24/98	101
6/25/98	101
7/15/98	44
7/17/98	43

Table 2. Estimates of $t(\lambda)\rho_w(\lambda)$ for low-*Chl* water.

λ (nm)	$[\rho_w(\lambda)]_N$	$t(\lambda)\rho_w(\lambda)$: $\tau_a(865) = 1.0$	$t(\lambda)\rho_w(\lambda)$: $\tau_a(865) = 1.8$
412	0.035	0.0100	0.0059
443	0.035	0.0121	0.0083
490	0.020	0.0080	0.0055
510	0.015	0.0063	0.0046
555	0.004	0.0019	0.0014

Table 3. Spectral values of the two imaginary parts of the refractive index used to create the set of dust models.

λ (nm)	Patterson [1981]	This Work
412	0.01200	0.0080
443	0.00910	0.0045
490	0.00795	0.0040
510	0.00734	0.0030
555	0.00540	0.0020
670	0.00430	0.0010
765	0.00316	0.0005
865	0.00120	0.0005

Table 4. Mean error in $\rho_A(\lambda)$ for the 40 images as described in the text.

λ (nm)	$\rho_A(\lambda)$
412	–0.0005
443	+0.0015
490	+0.0005
510	–0.0015
555	–0.0015
670	–0.0050
765	–0.0015

Table 5. Relationship between model name and number for Figures 7 and 8

Model name and vertical structure	Model number
BDW1 v02	1
BDW1 v04	2
BDW1 v06	3
BDW2 v02	4
BDW2 v04	5
BDW2 v06	6
BDW3 v02	7
BDW3 v04	8
BDW3 v06	9
BDS1 v02	10
BDS1 v04	11
BDS1 v06	12
BDS2 v02	13
BDS2 v04	14
BDS2 v06	15
BDS3 v02	16
BDS3 v04	17
BDS3 v06	18

Figures and Plates

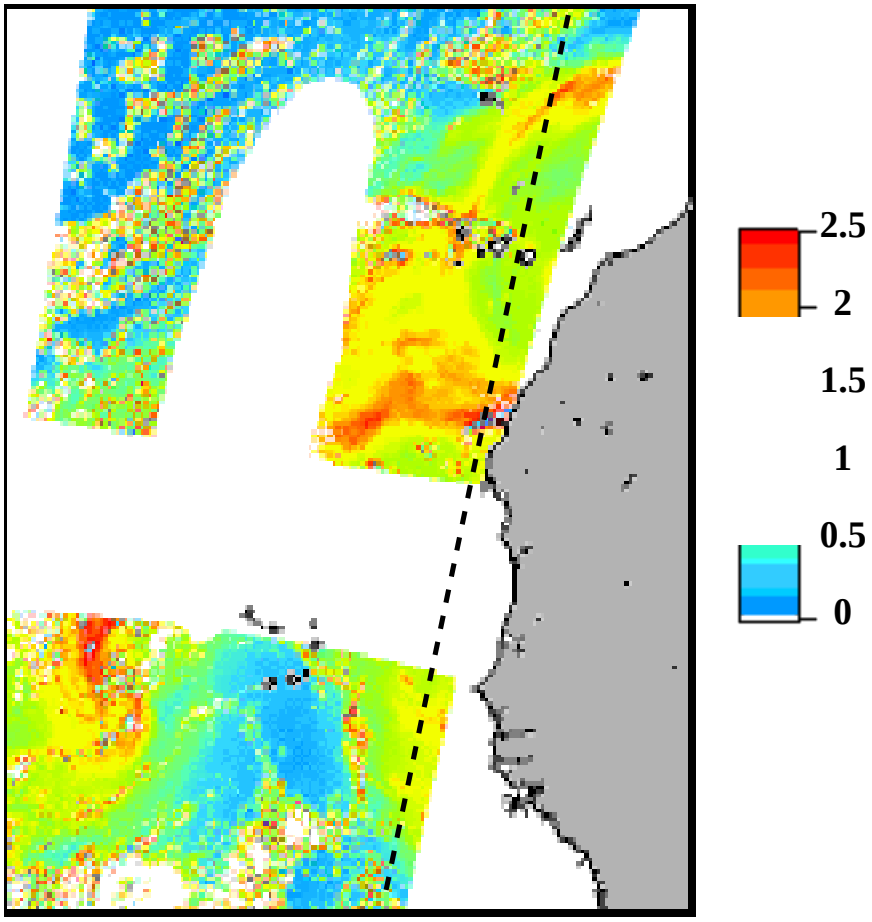

Plate 1. SeaWiFS image of $\rho_A(865)$ showing a huge dust plume on 23 June 1998. Reflectance is high for red colors and low for blue-purple. The vertical black area is the portion masked because of sun glint, and the horizontal strip is the data that is missing because of the change in the sensor's tilt from north to south.

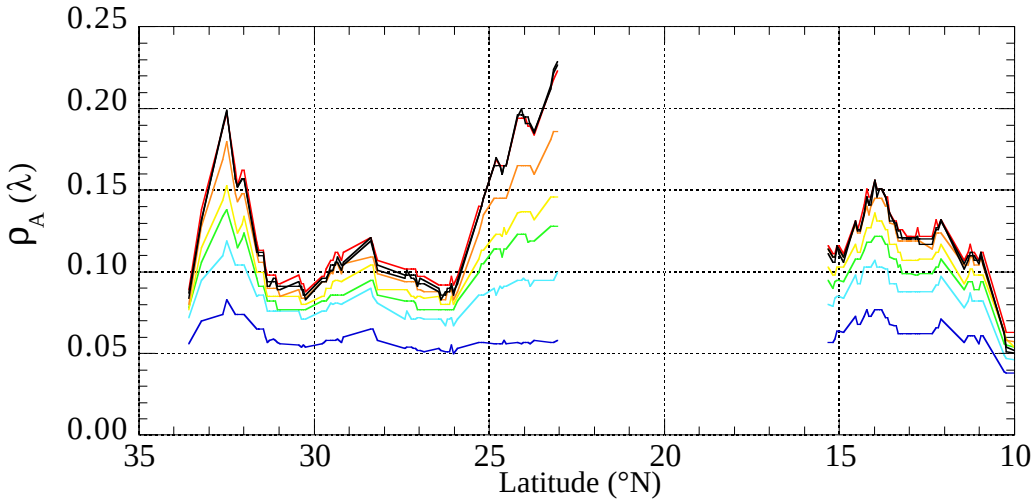

Figure 1. Extracted values of $\rho_A(\lambda)$ along the track line on Plate 1 as described in the text: Dark blue for 412 nm, light blue for 443 nm, green for 490 nm, yellow for 510 nm, orange for 555 nm, red for 670 nm, and black for 765 and 865 nm. Note that the quantity referred to as $\rho_A(\lambda)$ contains the water contribution, i.e., it is really $\rho_A(\lambda) + t(\lambda)\rho_w(\lambda)$.

Figure 2. (next page) Predicted $\rho_A(\lambda)$ along the track line on Plate 1 for different dust models (see text): (**a**) BDS1; (**b**) D5S; (**c**) MIS; (**d**) M90. See Figure 1 for color legend. Note that for the M90 model, we removed pixels with $\rho_A(865) > 0.15$ because the standard SeaWiFS Look-up Table that we used are not made to handle high aerosol optical depth.

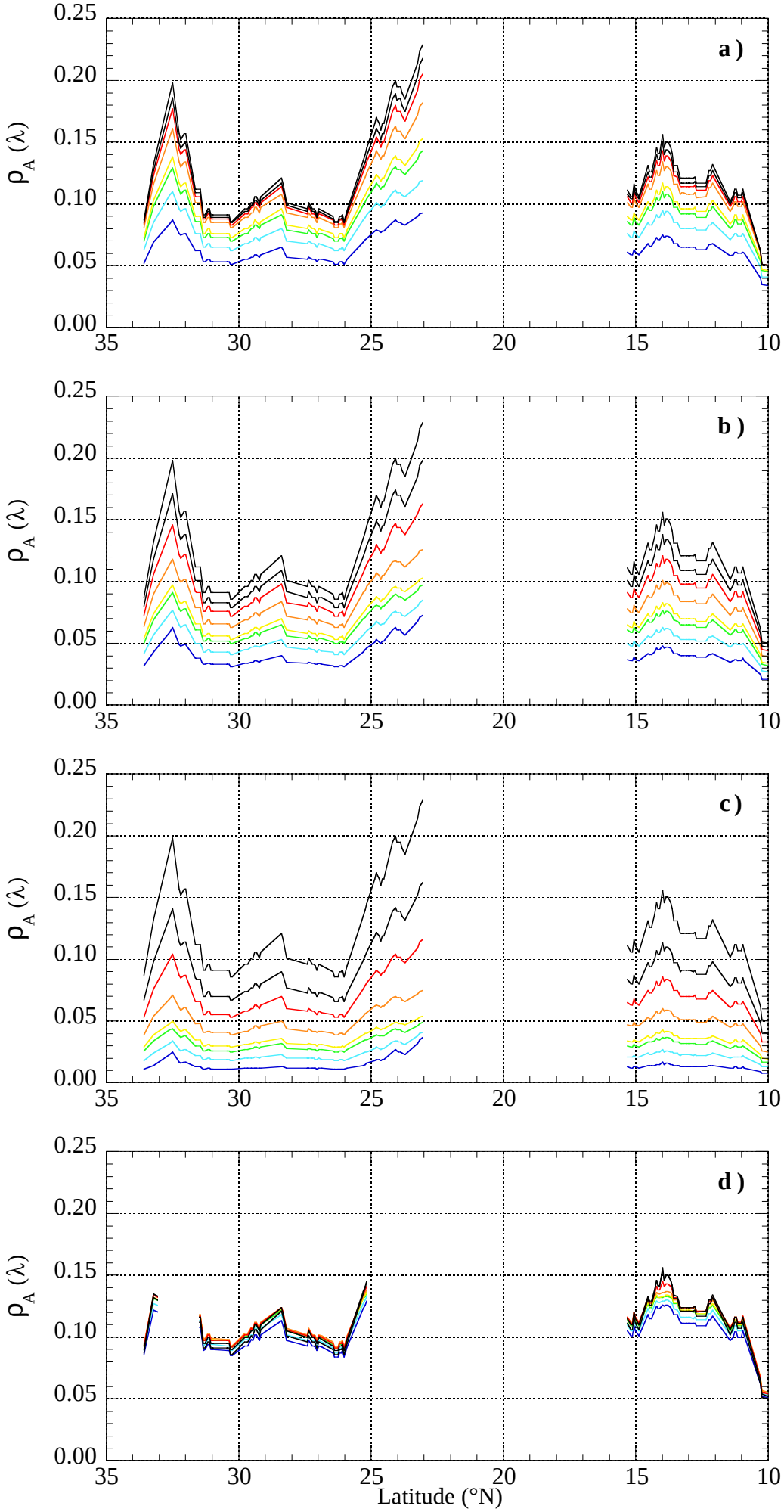
a)
b)
c)
d)
ρA (λ)
0.25
0.20
0.15
0.10
0.05
0.00
35
30
25
20
15
10
Latitude (°N)

a)

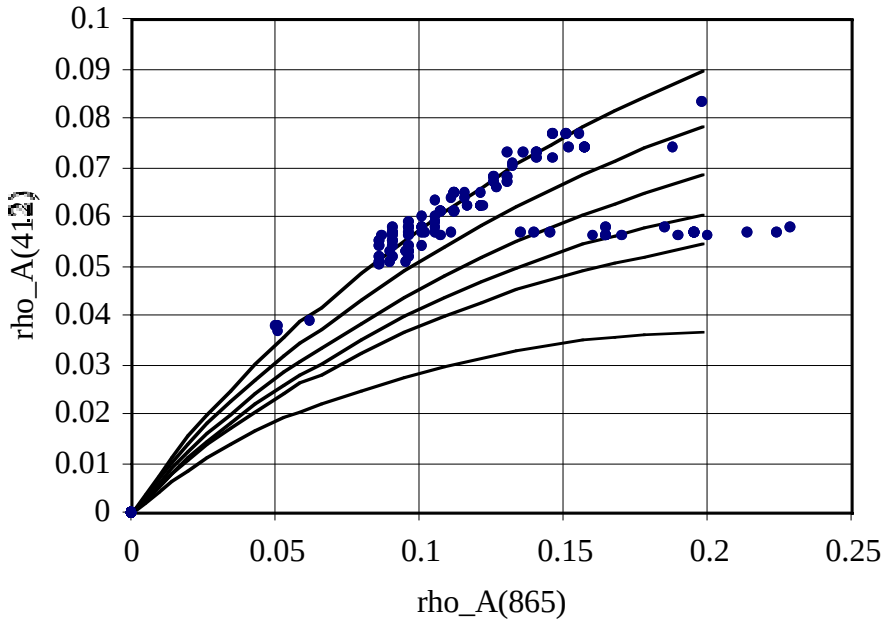

b)

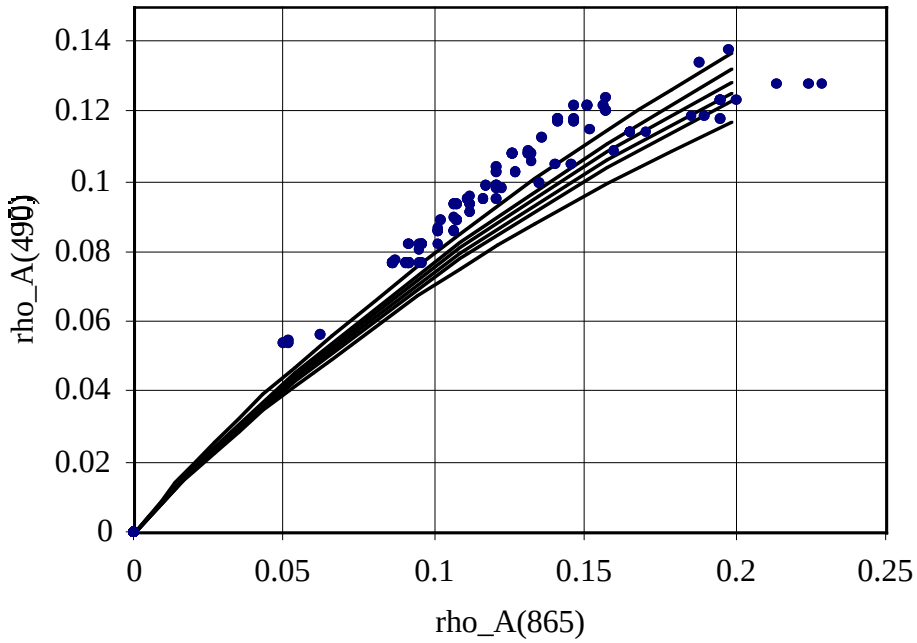

Figure 3. Comparison between the measured and computed (using the BDS1 model) relationship between (**a**) $\rho_A(412)$ and $\rho_A(865)$ and (**b**) $\rho_A(490)$ and $\rho_A(865)$ for various vertical structures of the dust layer (v00 through vUU) as described in the text. The v00 curve is on top, then v02, v04, v06, v08, and vUU is on bottom. Simulations were carried out for six values of the optical depth (0, 0.2, 0.5, 1.0, 1.5, and 2.0). Note that for measured dots, the quantity referred to as $\rho_A(412)$ (respectively $\rho_A(490)$) contains the water contribution, i.e., it is really $\rho_A(412) + t(412)\rho_w(412)$ (respectively $\rho_A(490) + t(490)\rho_w(490)$). The flat portion of the SeaWiFS data corresponds to the data between 23°N and 26°N in Figure 1.

a)

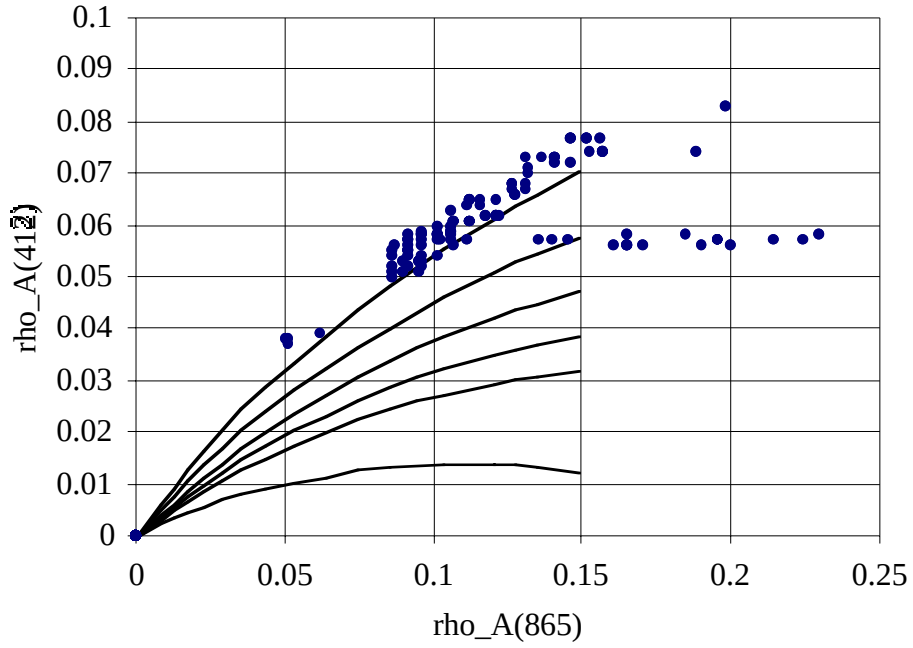

b)

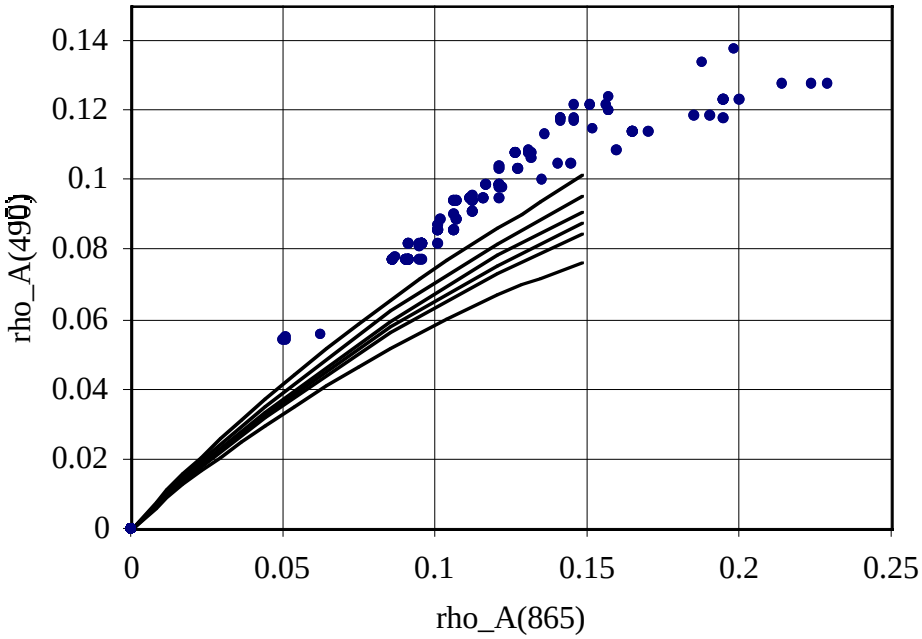

Figure 4. Same as Figure 3, but for the BDS3 model (see text). Note that the maximum value of $\rho_A(865)$, which is still computed for an optical depth of 2, is lower than that in Figure 3. This is due to the change of the dust phase function in the backward direction between the two models: the bigger particles, the smaller phase function and thus the smaller $\rho_A(865)$.

a)

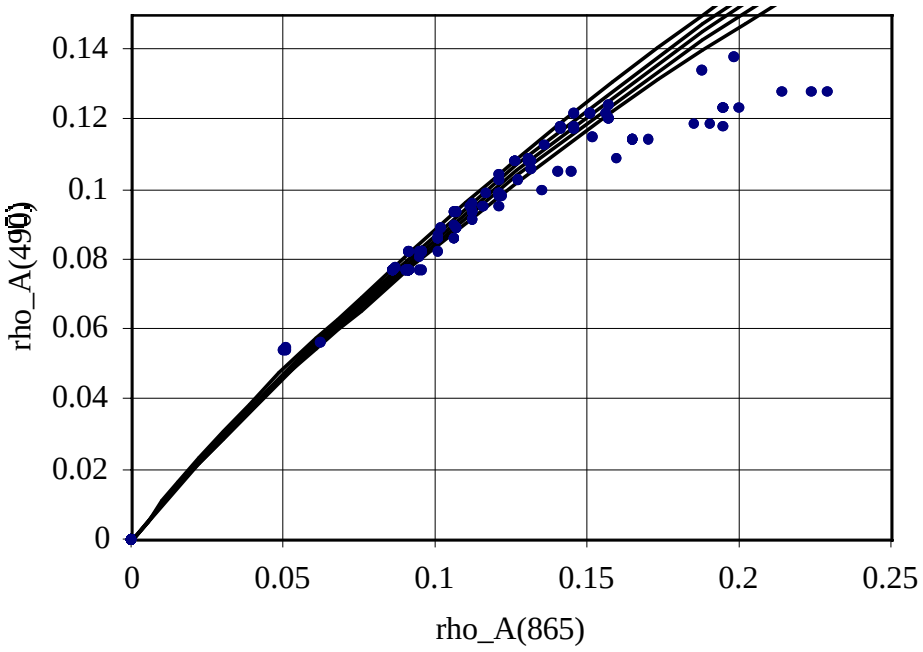

b)

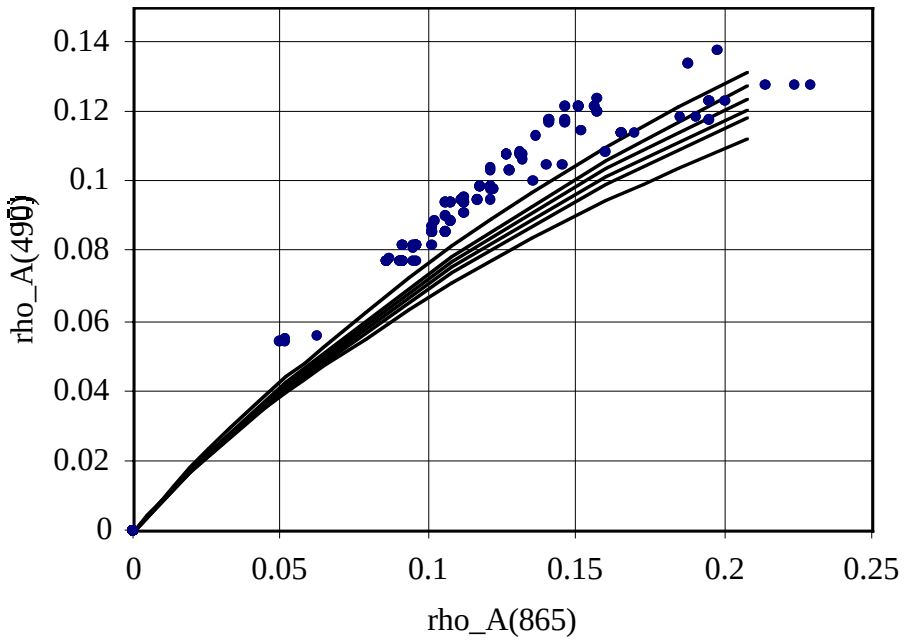

Figure 5. (**a**) Same as Figure 3b for the BDW 1 model; (**b**) Same as Figure 4b for the BDW 3 model.

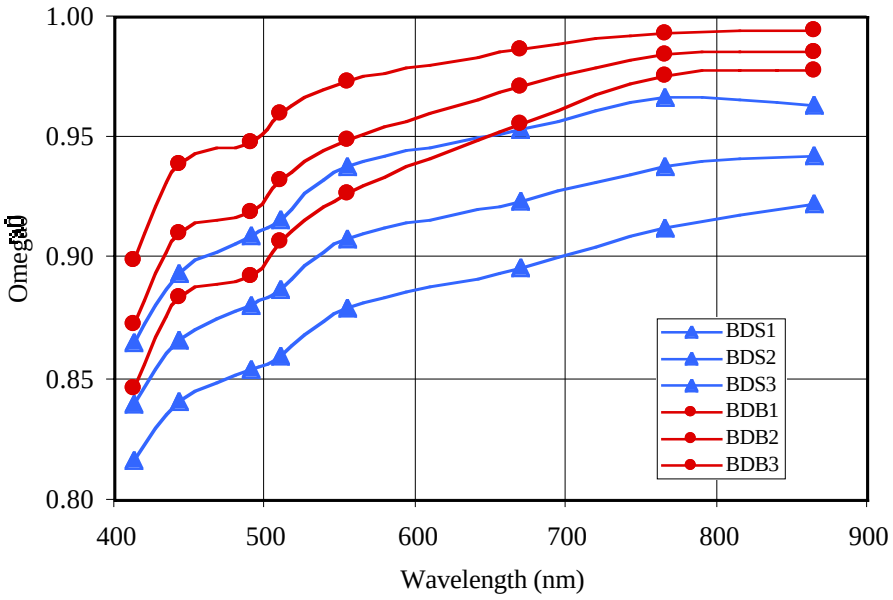

Figure 6. $\omega_0(\lambda)$ for the selected BDS and BDW models.

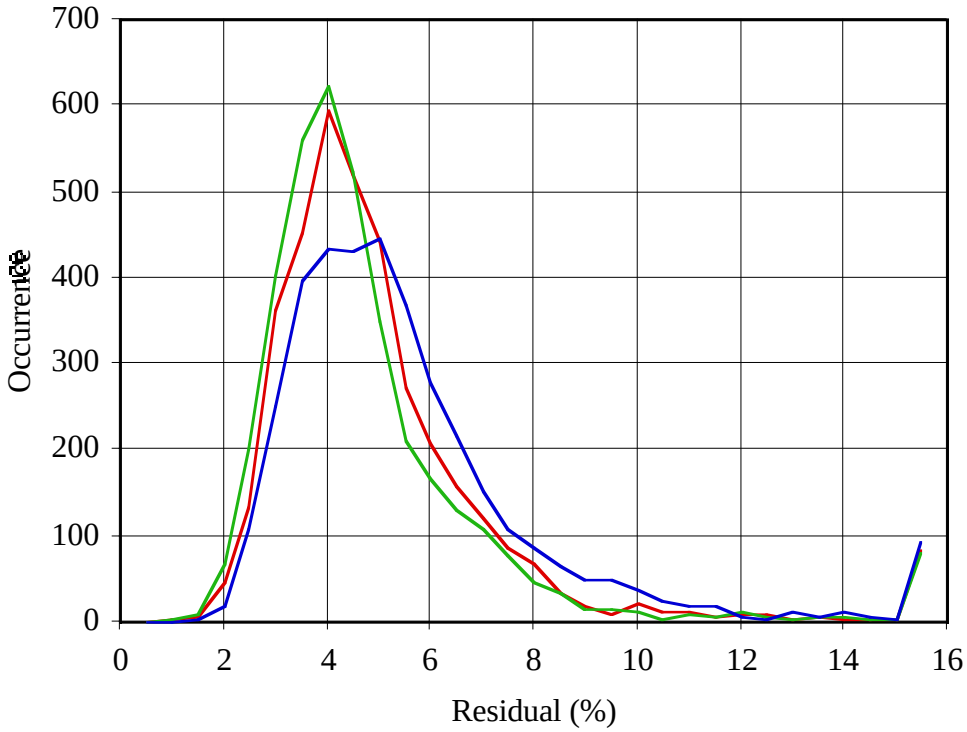

Figure 7. Number of occurrences of the residual error (%) for the 40 images using the procedure described in the text: The red curve is for the climatological *Chl* value, and the green and blue curves are for the "double *Chl*" and "half *Chl*" experiments respectively. The total number of pixels processed is of 3702 (see Table 1).

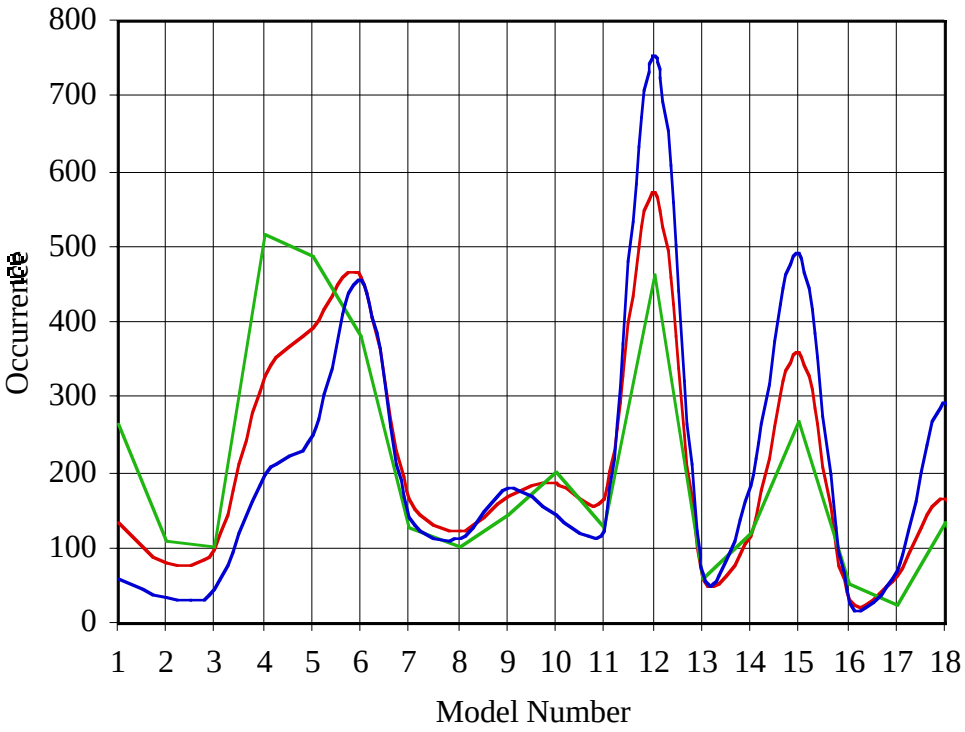

Figure 8. Number of occurrences for which a given model is chosen as "best" for the residuals shown in Figure 7. Colors are the same as in Figure 7. Model numbers are given in Table 3.

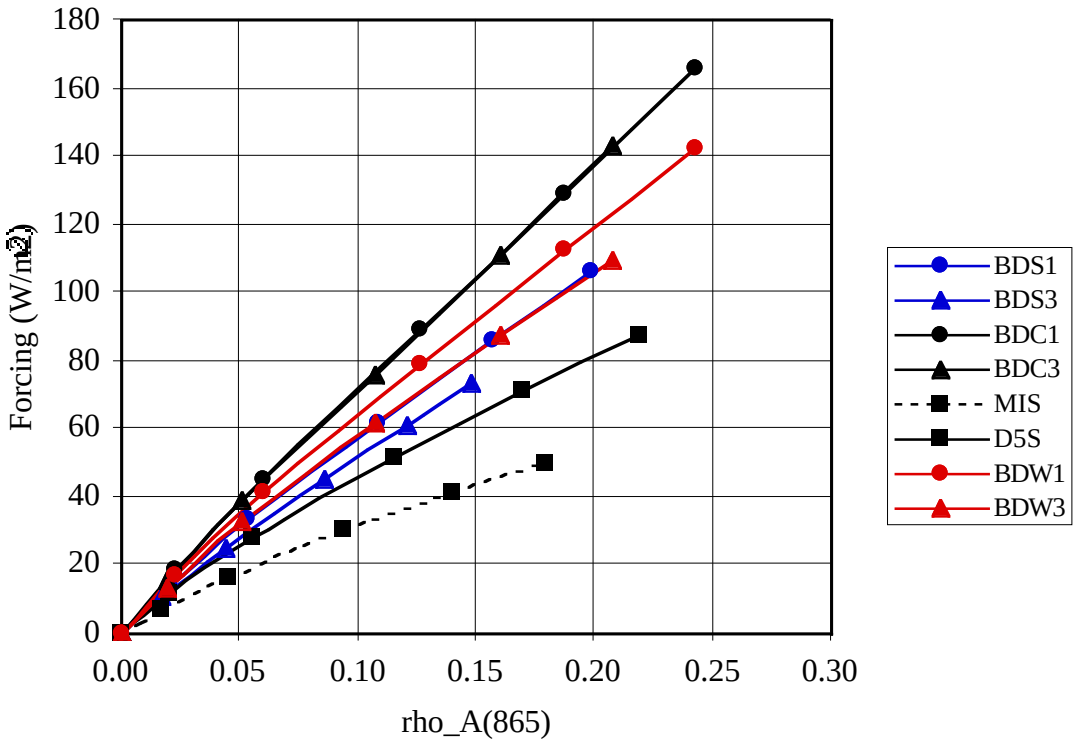

Figure 9. Instantaneous radiative forcing of several models for the spectral region 400-900 for the geometry of the track in Plate 1. The dust is assumed to be uniformly mixed with air from the surface to an altitude of 4 km. Data symbols correspond to $\tau_a(865) = 0, 0.2, 0.5, 1.0, 1.5,$ and 2.0.